IMPROVED METHODS FOR MONITORING ARTERIAL STIFFNESS AND BLOOD PRESSURE

By

Mingwu Gao

A DISSERTATION

Submitted to
Michigan State University
in partial fulfillment of the requirements
for the degree of

Electrical Engineering—Doctor of Philosophy

2016

ABSTRACT

IMPROVED METHODS FOR MONITORING ARTERIAL STIFFNESS AND BLOOD PRESSURE

By

Mingwu Gao

Cardiovascular diseases are the top 1 natural death cause in the United States. Proactive diagnosis and treatments can significantly reduce patient risk for cardiovascular diseases. Arterial stiffness and blood pressure is recognized as independent predictor of patients' cardiovascular events. They are probably the most commonly measured indictors of cardiovascular diseases. Arterial stiffness and blood pressure measured in a convenient and accurate manner can provide independent diagnosis information for better patient treatment. Blood pressures measurements have been deployed heavily in the area of hypertensive patient stratification. On the other hand, people use pulse wave velocity as a surrogate measurement of arterial stiffness due to unavailability of arterial stiffness measurement technique. In the past decades, arterial stiffness and pulse wave velocity have been proved to be an independent predictor of cardiovascular events. However, the measurements of blood pressure and arterial stiffness are still inadequate in accuracy, convenience and clinical relevance.

This dissertation reported four studies concerning improved methods for monitoring arterial stiffness and blood pressure. The first study proposed an improved technique to monitor arterial stiffness or evaluating Pulse Wave Velocity using arterial tube-load model for robust and accurate arterial stiffness estimation. The second study covers the technique of estimating pulse transit time as a function of blood pressure. This technique can potentially be employed to build calibration curve between pulse transit time and blood pressure using only baseline measure for continuous and cuffless blood pressure monitoring; meanwhile this technique gives a rise of

extra pulse transit time correlating with systolic blood pressure which can be potentially useful for patient stratification. The third study investigates two non-invasively pulse transit time measurement techniques as cuffless blood pressure trackers and compare them against invasively measured pulse transit time as reference. The fourth study discusses an evolved technique to build adaptive transform function to estimate central pressure waveform from peripheral blood pressure waveforms. This technique is to improve more clinical significant central blood pressure monitoring based on more accessible peripheral blood pressure waveform. In the end the summary and future work are given for future improvement in arterial stiffness and blood pressure monitoring.

To my parents, Guangzhi Gao and Lijun Liu

ACKNOWLEDGEMENTS

I would like to express my sincere appreciation to my advisor Dr. Ramakrishna Mukkamala for the chance working in the exciting area for my Ph.D. His guidance and support throughout my Ph.D. study inspired me to spare no efforts working toward this degree. His passion and love for great research also set a great yardstick for me to measure myself against.

I would like to thank my committee members Dr. Lalita Udpa, Dr. Prem Chahal and Dr. N. Bari Olivier for their valuable discussions during each of my presentation and their guidance for my study in the Ph.D. program. Special thanks are given to Dr. Olivier for his collaboration in a number of projects we worked together. The projects cannot be completed without him.

I would like to express my gratitude to my collaborators from institutes all over the world. To be specific, Hao-Min Cheng, Shih-Hsien Sung, Chen-Huan Chen from National Yang-Ming University; Barry Fetics and David A. Kass from Johns Hopkins Medical Institutions; William C. Rose from University of Delaware for their great effort in all aspects of the research projects.

I would like to extend my appreciations to my dear colleagues Federico Aletti, Xiaoxiao Chen, Guanqun Zhang, Mohsen Moslehpour, Jiankun Liu, Anand Chandrasekhar and Keerthana Natarajan for their help during my research and for the good times we spent together.

In addition, I would like to take this opportunity to thank all my friends for letting me share my joys and frustrations. Thank you so much for your company and emotional support. Life would have been tough without you.

In the end, I would like to express my gratitude to my Mum and beloved Dad for raising me up, supporting me and loving me unconditionally. It's been a rough but fun journey. I definitely enjoy it. I cannot be who I am without you. I don't know how to thank you more, Mum and Dad!

TABLE OF CONTENTS

LIST OF TABLES

LIST OF FIGURES

Chapter 1. Introduction

1.1 Backgrounds

The science and technology history has been mostly propelled by human beings' curiosity to understand ourselves and everything around, followed by the efforts to leverage the obtained knowledge for better wellbeing of all kinds. In this process, tremendous efforts were made to demystify the physiology of our body for the prevention and treatment of various diseases including cardiovascular related diseases. Unfortunately the progress made to harness cardiovascular related diseases remains far from enough. Diseases of heart itself attribute to 23.7% of the deaths and stance as the leading cause of death in the United States even with cancer taken into account [1]. Other vital diseases such as stroke, cerebral hemorrhage and kidney diseases can also potentially caused by the mortality of cardiovascular system. On the other hand, the proportion of the elderly population is growing as the clinical staff per capita declines [2] with a ~30% shortfall in nurses projected by 2020 [2]. These demographic changes accentuate the importance of effective continuous (i.e., automated), and less invasive (i.e., safer and simpler) patient monitoring systems especially for the hemodynamic monitoring of cardiovascular disease [3].

The function of the cardiovascular circulation is to serve the needs of body tissues by transporting essential substances to the tissues, removing waste products of metabolism, conducting hormones from one part of the body to another, and maintaining an appropriate environment in the tissue fluids of the body [4]. Due to the universal physical connectivity between cardiovascular system and organs in the body, any morbidity in cardiovascular system may cause morbidity or damage on organs such as heart, brain and kidney. Meanwhile the body's well-being and drug usage also heavily depend on the monitoring of hemodynamics.

Hemodynamics is a branch of hydraulics, and to the extent that it exists as a separate discipline, it owes its identity to the peculiar properties of blood and the vascular tree, which do not behave in accordance with the simplest forms of the relevant physical laws. Three different lines of interest converge in hemodynamics: the physical properties of the heart and blood vessels, the relation of these properties to the phenomena that are observed in the circulation, and the application of the results to physiological research or clinical medicine [5].

It is widely acknowledged that William Harvey's unequivocal description of the blood circulation symbolized the emergence of hemodynamics. For the centuries thereafter hemodynamics monitoring were advancing along two paralleled but interactive paths: a. Methods of Hemodynamic Measurement to obtain signal and information directly from measurements; b. Theories of Hemodynamics concerning theoretical, experimental as well as clinical principles of blood flow in arteries including analysis of hemodynamic measurements.

Thanks to the efforts of people working in this area generation after generation, a variety of hemodynamic measurements are currently available for clinical or research use such as blood pressure, blood flow, blood volume, heart volume, electrocardiogram (ECG), Impedance cardiography (ICG), Ballistocardiography (BCG) and so on. These signals range from invasive to noninvasive, from 1D to 2D, from electric based to acoustic, electromagnetic or even mechanical based. Meanwhile, hemodynamic theory has grown tremendously on the rise of development in math, physics, physiology as well as the invention and application of computers.

Among various cardiovascular diagnostic information extractable from available measurements, blood pressure and arterial stiffness are probably the most common measured indictors of cardiovascular diseases. Blood pressures measurements have been deployed heavily in the area of hypertension patient stratification. On the other hand, arterial stiffness is not easy

to measure and therefore people use pulse transit time as surrogate of arterial stiffness measurement. In the past decades, arterial stiffness and pulse wave velocity have been proved to be an independent predictor of cardiovascular events. However, the measurements of blood pressure and arterial stiffness are still inadequate in accuracy, convenience and clinical relevance.

In this dissertation, I reported the techniques and studies I conducted in the past years in an effort to improve blood pressure and arterial stiffness monitoring.

1.2 Organization

Chapter 2 reports an improved technique to monitor arterial stiffness or evaluating Pulse Wave Velocity using arterial tube-load model. Chapter 3 covers the technique of estimating pulse transit time as a function of blood pressure toward both ubiquitous blood pressure monitoring and better arterial stiffness indicator. Chapter 4 investigates two non-invasively measured pulse transit time as cuffless blood pressure trackers and compare them against invasively measured pulse transit time. Chapter 5 discusses an evolved technique to build adaptive transform function from peripheral blood pressure waveforms to central pressure waveform. This technique is to improve more clinical significant central blood pressure monitoring based on more accessible peripheral blood pressure waveform. In the end the summary and future work are covered in Chapter 6.

Chapter 2. Improved Pulse Wave Velocity Estimation Using an Arterial Tube-Load Model

2.1 Introduction

Pulse wave velocity (PWV) is the speed of energy wave transmission in the arteries. According to the Bramwell-Hill equation, PWV varies inversely with the square root of arterial compliance [6]. PWV indeed increases as the arteries stiffen with aging and disease [7][8][9]. PWV in the aorta is now the most important index of arterial stiffness for two reasons [10]. Firstly, it is an independent predictor of all-cause mortality and cardiovascular events in hypertensive and other patients [10][11]. Secondly, while direct measurement of arterial compliance involves nontrivial tracking of changes in vessel area and BP, PWV is easier to measure [10][12].

PWV is most easily determined as the ratio of the distance and pulse transit time (PTT) between central and peripheral arterial sites. Conventionally, PTT is estimated by measuring blood pressure (BP) or velocity (BV) waveforms at these sites with non-invasive tonometers or Doppler ultrasound probes and then detecting the foot-to-foot time delay between the waveforms. This foot-to-foot detection technique is also applicable to sequential measurements of the waveforms via a simultaneously measured ECG (i.e., ECG gating).

The foot-to-foot detection technique may be explained as follows. BP and BV waveforms arise as the superposition of transmitted and reflected waves. As a result, as shown in Figure 2-1a [13], they vary in shape throughout the arterial tree. If wave reflection were absent, a pair of BP (or BV) waveforms would mainly differ by just a time delay equal to PTT, whereas a pair of BP and BV waveforms would likewise differ by the time delay as well as a scale factor (equal to the arterial area times the characteristic impedance) [13]. Hence, the premise of this technique is that interference from the reflected wave is negligible during late diastole and early systole.

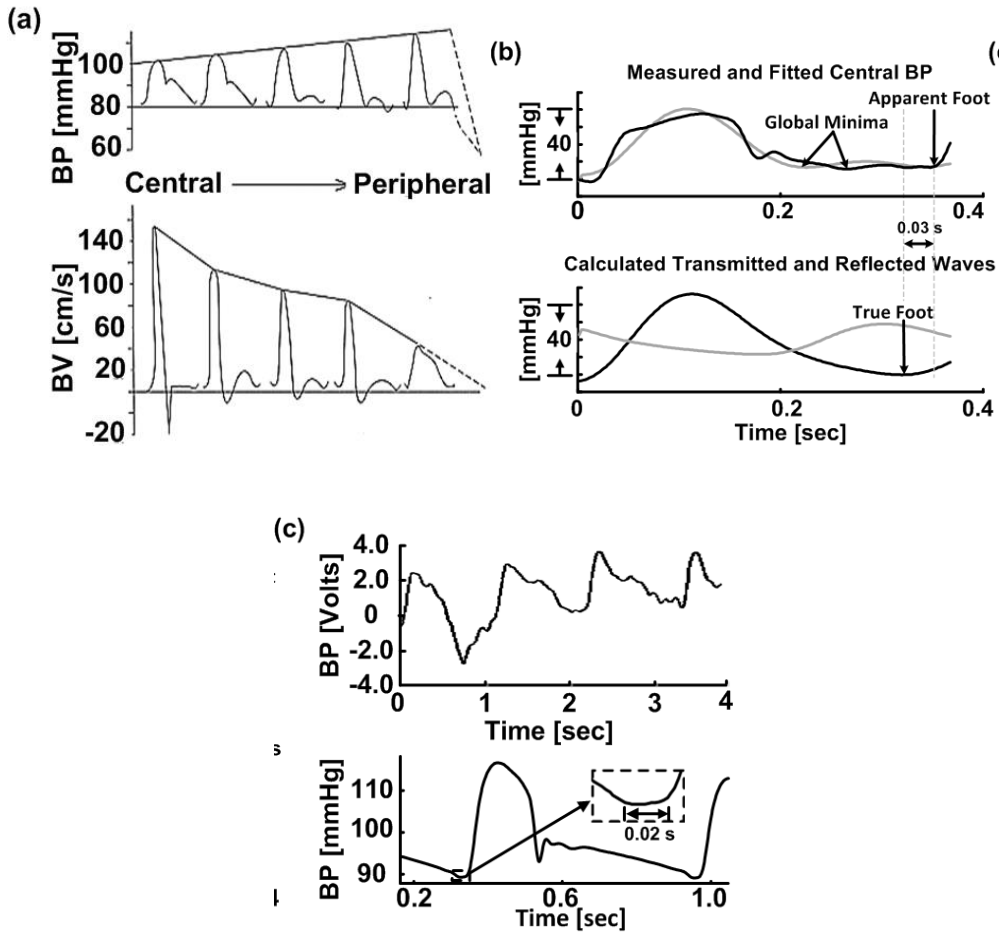

Figure 2-1 The conventional foot-to-foot detection technique for pulse transit time (PTT) estimation is prone to error due to wave reflection interference and waveform artifact.

(a) Blood pressure and velocity (BP and BV) waveforms arise as the sum of transmitted and reflected waves. As a result, these waveforms vary in shape throughout the arterial tree. Hence, the premise of the technique is that wave reflection interference is negligible at the waveform feet. Adapted from (Nichols 2005, book) . (b) Measured and fitted central BP waveforms (upper) and calculated transmitted and reflected waves in the central aorta (lower) during tachycardia. The reflected wave (gray) is actually prominent near the waveform feet such that the apparent (central BP) foot deviates from the true (transmitted wave) foot. (c) Detection of the foot is often difficult due to non-invasive waveform artifact (upper) (Boutouyrie 2010) and can be subjective even for invasive waveforms (lower) (Milnor 1982). Just a 0.01 sec error in foot detection can result in a pulse wave velocity (PWV) error of ~15% of the entire PWV range (Boutouyrie 2010, Sugawara2010).

However, wave reflection interference around the waveform feet can become nontrivial with changes in heart rate (HR) [14]. For example, during tachycardia, the time delay between the forward and backward waves in the central aorta is a large fraction of the cardiac cycle length. Hence, as shown in Figure 2-1b, the backward wave may be prominent near the central BP waveform foot. Further, the relative magnitude of wave reflection increases with peripheral resistance [13][15]. Just as important, since the technique restricts its analysis to one pair of waveform samples per cardiac cycle, it is not robust to motion and other artifact often present in the non-invasive waveforms, as shown in Figure.2-1c [16]. In fact, detection of the foot can be subjective even for invasive waveforms during normal conditions (Figure 2-1c) [5].

Even seemingly small detection errors caused by wave reflection interference and/or artifact can result in serious PWV errors. For example, using average adult values of 0.5 m and 0.06 s for the distance and PTT between carotid (central) and femoral (peripheral) arteries [17][18], just a 0.01 s error in foot detection, which is not uncommon (Figure 2-1c), yields a PWV error of about 1.4 m/s. This error magnitude is of concern, as the physiologic range of PWV is, for the most part, only from about 6 to 16 m/s [17]. Indeed, a 1 m/s change in PWV has been shown to increase the risk of mortality by 39% and to yield an adjusted relative risk for mortality of 0.71 in end-stage renal disease patients [19][20].

Hence, while the conventional technique does yield PWV estimates with predictive value, it also produces errors that carry clinical consequences. Three examples follow.

First, PWV and BP often show positive correlation. In fact, PWV is frequently advocated as a way to achieve continuous, non-invasive, and cuff-less BP monitoring [21][22][23][24]. The mechanism is well known. Increases in BP cause decreases in arterial compliance, as slack

collagen fibers become stiffer. The arterial compliance decreases, in turn, cause increases in PWV as per the Bramwell-Hill equation. While changes in vasomotor tone could also acutely modulate arterial compliance, this effect is less of a factor in large arteries wherein smooth muscle is relatively sparse [25]. However, plots of BP versus PWV typically show excessive scatter about the line of best fit even under general anesthesia wherein changes in vasomotor tone are minimal [21]. As shown herein, this scatter can be reduced with improved analysis techniques.

Second, arterial elastic modulus, which is another more difficult-to-measure index of arterial stiffness, does not change by increasing HR [26]. Yet, PWV was shown to increase with atrial pacing-induced increases in HR despite no change in BP or other relevant variables [27]. This finding, which suggests the need for a HR correction of PWV for risk stratification [27], must be due to error in estimating PWV [28] caused by progressive wave reflection interference (Figure 2-1b).

Third, several studies that have compared PWV to arterial compliance and other more difficult-to-measure indices of arterial stiffness have shown that PWV is of inferior clinical value. In one study, arterial compliance discriminated the severity of coronary artery disease, which is strongly associated with large artery stiffness, better than PWV [29]. In another study, arterial elastic modulus discriminated arterial stiffness patients from healthy subjects better than PWV ($p < 0.0001$ vs. $p = 0.004$) [30]. In a third exemplary study, arterial elastic modulus afforded a greater odds ratio for predicting all-cause mortality in end-stage renal disease patients than PWV (9.2 vs. 5.4) [19][31]. Hence, improving the accuracy of estimating PWV could enhance its predictive value.

In this study, we conceived techniques for improved PWV estimation from central and peripheral BP and/or BV waveforms. These techniques effectively estimate PWV from the entire waveforms, rather than just their feet, by mathematically eliminating the reflected wave via an arterial tube-load model. In this way, the techniques may be robust to artifact while revealing the true PWV (i.e., PWV in absence of wave reflection). Further, they may be applied to sequential waveform measurements via a simultaneously measured ECG. We tested these techniques in terms of the ability of their PWV estimates to track large changes in BP in anesthetized animals. Our results show superior BP-PWV correlation than the conventional technique. Preliminary versions of this study have been reported in abbreviated form [3][32].

2.2 Arterial Tube Load Model Based PWV Estimation Techniques

The techniques are illustrated in Figures.2-2 and 2-3 and are implemented in four steps. First, arterial transmission and reflection are represented with a tube-load model that has been shown to have excellent predictive value in other applications (see Discussion section) [33][34][35][36]. Second, the transfer function coupling measured central and peripheral BP and/or BV waveforms is defined in terms of the unknown model parameters. The parameters represent the true PTT, peripheral resistance and compliance, and possibly the characteristic impedance times the arterial area. Third, all parameters are estimated by finding the transfer function, which when applied to one of the waveforms, optimally fits the other. Fourth, PWV is calculated from the PTT estimate. Below, we describe the techniques and a way to augment the computational speed in implementing them.

2.2.1 PWV Estimation from Simultaneous Measurements

The arterial tree is modeled as m parallel, uniform tubes with terminal loads, as shown in Figure 2-2a. The i^{th} tube (i = 1, …, m) represents the wave travel path between the central aorta and the i^{th} peripheral artery. Each tube is frictionless and thus has constant characteristic impedance

$$Z_{ci} = \sqrt{\frac{\rho L_i}{A_i C_i}}, \tag{2.1}$$

where L_i, A_i, and C_i are large artery length, area, and compliance while ρ is the blood density, and allows waves to travel along the tube with constant PTT

$$T_{di} = \sqrt{\frac{\rho L_i C_i}{A_i}} \tag{2.2}$$

[33][34][37]. The i^{th} load represents the arterial bed distal to the i^{th} peripheral artery. Each load has frequency-dependent impedance $[Z_i(\omega)]$ characterized by peripheral resistance $[r_i]$ and compliance $[c_i]$ while matching Z_{ci} at high frequency [33][34][37].

This model may be explained as follows. Cardiac ejection initiates pressure and velocity waves that travel from left to right along a tube. These forward waves move without distortion and are proportional to each other (via a characteristic impedance time arterial area scale factor). The waves are reflected in the opposite direction at the terminal load with relative magnitude and phase based on frequency according to the wave reflection coefficient

$$\Gamma_i(\omega) = \frac{Z_i(\omega) - Z_{ci}}{Z_i(\omega) + Z_{ci}} = \frac{r_i c_i}{r_i c_i + 2Z_{ci} c_i + j\omega 2 r_i c_i Z_{ci} c_i}. \tag{2.3}$$

The backward pressure and velocity waves likewise travel along the tube without distortion and are proportional to each other. The actual BP (or BV) waveform at any point on the tube may

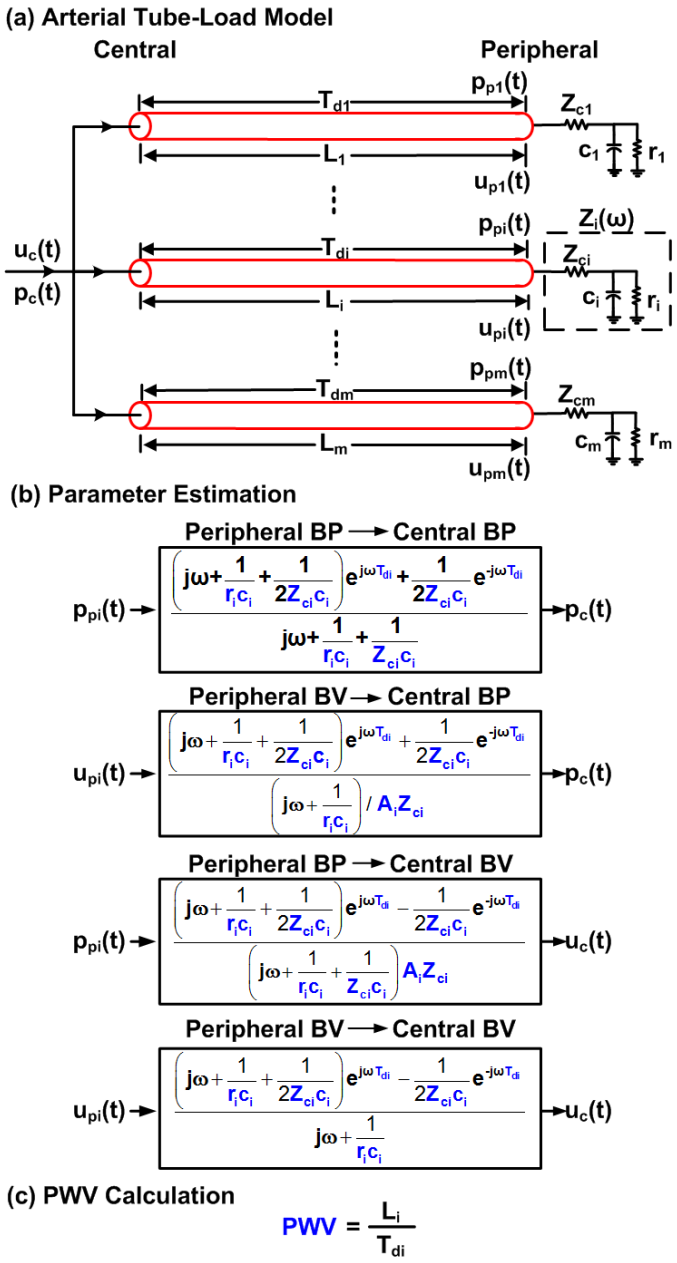

Figure 2-2 Arterial tube-load model-based technique for estimating PWV from simultaneously measured central and peripheral BP and/or BV waveforms.

thus be expressed as the sum (or difference) of the forward and backward pressure (or velocity) waves after time shifting to account for the wave travel time (as determined with PTT). In this way, the model mimics the progressive distortion that experimental BP and BV waveforms undergo with increasing distance from the heart (see Figure 2-1a). Also, from these expressions,

transfer functions relating a pair of BP and/or BV waveforms at any points on the tube may be defined in terms of the model parameters.

In particular, the transfer functions relating a peripheral BP or BV waveform [$p_{pi}(t)$ or $u_{pi}(t)$] to a central BP or BV waveform [$p_c(t)$ or $u_c(t)$] may be defined in terms of T_{di}, r_ic_i, $Z_{ci}c_i$, and possibly A_iZ_{ci}, as shown in Figure 2-2b. (The central waveform is regarded as the output here to increase computational speed, as described below.) These three or four parameters are estimated by finding the transfer function, which when applied to the former waveform, best fits the latter waveform in the least squares sense. This optimization is achieved via a numerical search, as described below. PWV is then computed from the T_{di} estimate and the distance between the two arterial measurement sites [L_i], as shown in Figure 2-2c. (Note that only the parameters characterizing a single tube and load are relevant; however, the parallel tube-load model is shown in Figure 2-2a to better indicate the physical meaning of the relevant tube and load.)

2.2.2 PWV Estimation from Sequential Measurements

An ECG is simultaneously obtained during sequential measurements of the central and peripheral waveforms [x(t) and y(t), which represent any of the input-output pairs shown in Figure 2-2b]. Then, an impulse train [$r_x(t)$] is formed from the segment of the ECG obtained during the x(t) measurement by placing unit impulses at the R-wave locations, as shown in Figure 2-3a [38]. (Note that the R-wave is generally straightforward to detect due to its relatively high frequency characteristic, and effective R-wave detection techniques are available [39].) Next, an impulse response [$h_x(t)$] is identified, which when convolved with $r_x(t)$, best fits x(t) in the least squares sense, as indicated in Figure 2-3b [38]. This optimization is achieved in closed-form via autoregressive exogenous input (ARX) identification [40]. Next, this analysis is repeated for the y(t) measurement to yield an impulse response relating $r_y(t)$ to y(t) [$h_y(t)$], as

shown in Figure 2-3ab. The impulse responses $h_x(t)$ and $h_y(t)$ represent x(t) and y(t) in response to the same cardiac excitation (i.e., a single, average cardiac contraction). Consequently and finally, the appropriate technique in Figure 2-2b is applied to $h_x(t)$ and $h_y(t)$ (instead of x(t) and y(t)), as indicated in Figure 2-3cd.

2.2.3 Implementation to Augment Computational Speed

The three or four unknown model parameters (i.e., T_{di}, r_ic_i, $Z_{ci}c_i$, and possibly A_iZ_{ci}) of the transfer functions in Figure 2-2b are estimated by searching over a physical range of candidate parameter sets. That is, the output is predicted by applying the transfer function to the input for each candidate set of parameters. The parameter set that yields the minimum mean squared error between the predicted and measured output is then selected as the final estimate. This numerical search generally produces the optimal solution but is computationally expensive. Its speed is augmented as follows.

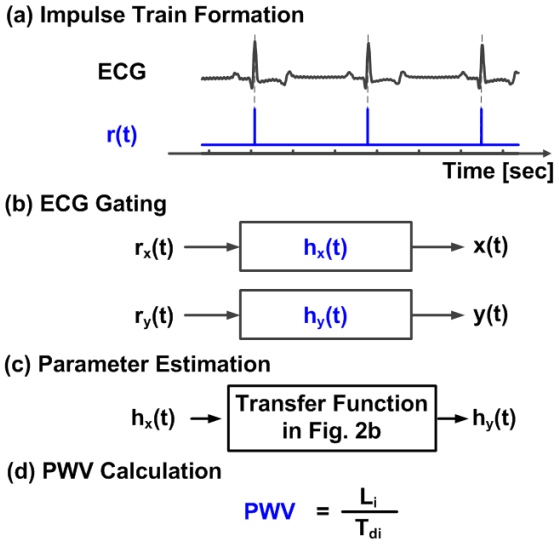

Figure 2-3 Arterial tube-load model-based technique for estimating PWV from sequentially measured central and peripheral BP and/or BV waveforms.
Here, x(t) and y(t) are any of the input-output pairs in Figure 2-2b.

Firstly, the number of candidate parameter sets is reduced. More specifically, since large artery characteristic impedance is often much smaller than peripheral resistance [13], the following constraint is employed: $0 < Z_{ci}c_i < r_ic_i$. Further, the T_{di} parameter is confined to be within a range established by the foot-to-foot detection technique.

Secondly, the number of search dimensions is reduced when A_iZ_{ci} is an unknown parameter. In particular, if the other three parameters were known, A_iZ_{ci} or its reciprocal is a linear parameter in the transfer function. Hence, for each candidate T_{di}, r_ic_i, and $Z_{ci}c_i$, this remaining parameter is computed in closed-form via the linear least squares solution.

Thirdly, the number of transfer function applications (i.e., convolutions) is reduced. The idea is to apply the transfer function in parts according to how it was derived (i.e., by adding or subtracting forward and backward waves after time shifting to account for their wave travel time). More specifically, first, the forward wave at the terminal load is computed by applying the transfer function $1/(1+\Gamma_i(\omega))$ to the peripheral input for each candidate r_ic_i and $Z_{ci}c_i$. The key point here is that this transfer function is not parameterized by T_{di}. Then, the backward wave at the terminal load is computed by either subtracting the forward wave from the measured peripheral BP input or subtracting the measured peripheral BV input from the forward wave. Next, the forward wave is advanced in time and the backward wave is delayed in time, both by T_{di}, for each candidate T_{di}. Then, the time shifted waves are either added to predict the central BP output (exactly or to within an A_iZ_{ci} scale factor) or subtracted to predict the central BV output (exactly or to within a $1/A_iZ_{ci}$ scale factor). In this way, the transfer function applications are performed only over a two-dimensional space (defined by r_ic_i and $Z_{ci}c_i$) rather than a three-dimensional space (defined by T_{di}, r_ic_i, and $Z_{ci}c_i$).

Finally, the speed in executing the search is increased by parallel computation. That is, the mean squared error between the predicted and measured output is computed for multiple candidate parameter sets at a time using multiple processors.

2.3 Technique Evaluation

We applied the new and conventional techniques to invasive BP and BV waveforms from animals during wide changes to BP. We evaluated and compared the techniques in terms of the ability of their PWV estimates to track BP in each subject. We provide details below.

2.3.1 Experimental Data

We collected data from six healthy adult beagles (10-12 kg) under an experimental protocol approved by the Michigan State University All-University Committee on Animal Use and Care. For each dog, we induced and maintained general anesthesia using an intravenous injection of propofol (2.2– 6.6 mg/kg) and an inhaled mixture of oxygen and isoflurane (1.5–2.5%). We inserted a micromanometer-tipped catheter (Millar Instruments) percutaneously into a femoral artery for a peripheral BP waveform. We likewise inserted a similar catheter into the opposite femoral artery and used fluoroscopic guidance (GE) to position it in the aorta for a central BP waveform. We placed a catheter in a cephalic vein for drug and fluid infusions as well as other instruments to address different specific aims. We interfaced all analog transducer outputs to a personal computer via a data acquisition system (DataQ Instruments). We then recorded the measurements at a sampling rate of 500 Hz during a baseline period and infusions of dobutamine, phenylephrine, and nitroprusside in three of the dogs and esmolol and saline in the remaining dogs. We used several infusion rates for each intervention and allowed recovery periods between the interventions.

We also studied two datasets previously collected from healthy animals under general anesthesia. The data collection procedures were approved by institutional animal care committees and are described in detail elsewhere [35][41]. One dataset included central (ascending aorta) and peripheral (femoral artery) BP waveforms via micromanometer-tipped catheters, along with surface ECGs, from six dogs (10-12 kg adult beagles) during a baseline period and hemodynamic drug infusions, blood volume changes, and cardiac pacing. The other dataset consisted of a central (ascending aorta) blood flow waveform via an ultrasonic flow probe and a peripheral (femoral artery) BP waveform via a fluid-filled catheter from five swine (30-34 kg) before and after the infusion of hemodynamic drugs and blood volume changes. The waveforms were available at a sampling rate of >250 Hz.

Importantly, isoflurane was used to achieve a deep plane of anesthesia in all 17 animals. Isoflurane is a potent vasodilator and severely blunts cardiovascular reflexes [42]. Indeed, the animals were hypotensive at baseline, and there was little HR response to the vasoactive drug infusions and blood volume changes. So, both basal vasomotor tone and changes in vasomotor tone were minimal. As a result, the acute BP changes served as a particularly useful reference for PWV estimates in this study. However, there was one exception in the dog in which low rate cardiac pacing was performed. As the pacing rate was decreased to 25 bpm, severe hypotension ensued. Under this dire situation, peripheral resistance, which was measured using a femoral artery blood flow probe that happened to be placed in this particular dog [35], increased reflexively perhaps due to a central ischemic response. We therefore excluded the data during the low rate cardiac pacing, which was last intervention performed in this dog.

2.3.2 Data Analysis

With these data, we were able to assess the new techniques as applied to (a) simultaneous central and peripheral BP waveforms, (b) sequential central and peripheral BP waveforms, and (c) simultaneous central BV and peripheral BP waveforms. We obtained the central BV waveform by dividing the central blood flow waveform by the nominal aortic cross-sectional area of the swine.

For the simultaneous measurements, we applied the techniques to estimate PWV for each beat of the waveforms. We then averaged the PWV estimates over 15-sec intervals.

For the sequential measurements, we applied the technique to 15-sec intervals of the waveforms to obtain a PWV estimate. For the ARX identification step, we set the autoregressive and moving average orders to the number of samples between the R-wave and the peak of the BP waveform. We determined this order empirically. For the tube-load model parameter estimation step, we used one beat length of the impulse responses, as they should eventually converge to the same exponential diastolic decay [41]

For comparison, we applied the foot-to-foot detection technique to estimate average PWV over 15-sec intervals from the same waveform pairs. We specifically implemented all of the automatic foot detection methods in [43][44] including a recently proposed diastole-patching method [45] and settled on the tangent line intersection method, as it performed best overall. (Note that the diastole-patching method performed similarly to this method as applied to the BP waveforms but is not applicable to BP and BV waveforms [45].)

We evaluated the PWV estimates of each technique in terms of their ability to track diastolic and mean BP in particular. In theory, the PWV estimates of the conventional technique should track

diastolic BP best by virtue of being derived from the waveform feet, whereas the PWV estimates of the new techniques should correlate best with mean BP by virtue of arising from all waveform samples. First, we measured the average diastolic and mean BP over 15-sec intervals. Then, we found the line of best fit between the PWV estimates of a technique and one of the measured BP parameters for each subject. (Note that use of higher order polynomials did not materially improve the fit.) We used the resulting correlation coefficient between the PWV estimates and measured BP parameters as one evaluation metric. Next, we predicted each BP parameter from the corresponding PWV estimate and best-fit-line. Finally, we computed the root-mean-squared-error (RMSE) between the predicted and measured BP parameters for another evaluation metric. (Note that we used the same data for determining the line of best fit and computing the RMSE, as our goal was to establish the ability of the PWV estimates to track the BP parameters rather than the capacity of the best fit line to predict BP parameters from PWV estimates. Further, we employed this procedure for all techniques to obtain a fair comparison.)

We statistically compared the correlation coefficients and RMSEs of the techniques. We specifically applied paired t-tests to compare the subject average metrics after log transformation to make the data more normally distributed.

2.4 Results

Table 1 shows the mean and standard deviation for diastolic and mean BP in each subject. The average standard deviation was 16±8 mmHg, so BP usually changed appreciably in each subject. If the BP changes were trivial, then a meaningful assessment of the techniques could not have been obtained in terms of tracking BP in each subject.

Figure 2-1b shows a sample of the measured and fitted central BP waveforms and estimated forward and backward waves in the central aorta from simultaneous central and peripheral BP

waveforms from a dog during high rate cardiac pacing. The foot of the measured waveform is ambiguous (e.g., there are multiple local minima). The forward and backward waves, which are buttressed by the agreement between the fitted and measured waveforms, indicate that wave reflection is the main cause of the ambiguity. That is, the backward wave is prominent during late diastole and early systole. As a result, the foot of the central BP waveforms, relative to the foot of the forward wave (i.e., the true foot), is to the left (when defined as the global minimum) or right (when defined as the initial, steep BP rise). This example suggests that the arterial tube-load model-based techniques can mitigate wave reflection interference.

Figure 2-4 illustrates sample plots of mean BP versus the PWV estimates from simultaneous and sequential central and peripheral BP waveforms from Dog 3, while Figure 2-5 shows sample plots of mean BP versus the PWV estimates from simultaneous central BV and peripheral BP waveforms from Pig 2. The arterial tube-load model-based techniques and the foot-to-foot detection technique showed the expected positive correlation between MAP and PWV. However, the new techniques exhibited noticeably reduced scatter about the line of best fit compared to the conventional technique. Note that this latter technique performed about the same for simultaneous and sequential measurements.

Tables 2-4 illustrate the quantitative results for each subject. For the simultaneous central and peripheral BP waveforms from dogs, the arterial tube-load model-based technique was able to reduce the average of the RMSEs by 35% and increase the average of the correlation coefficients by 11% relative to the foot-to-foot detection technique. These differences were all statistically significant. For the sequential central and peripheral BP waveforms from dogs, the new technique was able to decrease the average of the RMSEs by30% and increase the average of the correlation coefficients by 4% compared to the conventional technique. These differences were

Table 1 Subject-by-Subject Blood Pressure (BP) Statistics.

Dog	1	2	3	4	5	6	7	8	9	10	11	12	Average
Diastolic BP [mmHg]	77±29*	63±7	71±20	60±7	74±20	74±27	63±16	76±14	69±15	59±8	55±3	61±5	67±14
Mean BP [mmHg]	99±37	87±11	92±25	79±7	99±27	92±32	82±20	99±17	90±19	79±9	74±5	81±6	87±18

Pig	1	2	3	4	5	Average
Diastolic BP [mmHg]	48±15	66±18	64±12	62±16	56±16	59±15
Mean BP [mmHg]	59±18	85±21	85±16	81±20	73±20	77±19

*: Mean ± Standard Deviation

Table 2 Subject-by-Subject Results for Simultaneous Central and Peripheral BP Waveforms from Dogs

RMSE [mmHg]	Dog	1	2	3	4	5	6	7	8	9	10	11	12	Average
Diastolic BP	Foot-to-Foot Detection	5.3	3.5	4.9	5.9	8.5	12	4.1	2.4	6.5	2.6	2.2	4.3	5.2
	Arterial Tube-Load Model	5.2	2	2.4	4.3	3.8	5.1	3.8	3.3	4.6	2.4	1.4	2.2	3.4*
Mean BP	Foot-to-Foot Detection	5.6	4.7	5.3	4.0	8.7	14.1	4.3	2.6	8.3	3.2	3.2	5.3	5.8
	Arterial Tube-Load Model	4.1	3.8	2	3.4	7.2	5.4	3.1	3.3	5.1	2.9	2.1	3.3	3.8*
Correlation [unitless]	Dog	1	2	3	4	5	6	7	8	9	10	11	12	Average
Diastolic BP	Foot-to-Foot Detection	0.983	0.877	0.968	0.438	0.903	0.897	0.959	0.981	0.904	0.94	0.757	0.321	0.827
	Arterial Tube-Load Model	0.984	0.945	0.993	0.763	0.982	0.982	0.972	0.969	0.955	0.947	0.899	0.877	0.939**
Mean BP	Foot-to-Foot Detection	0.988	0.911	0.977	0.842	0.948	0.900	0.970	0.987	0.896	0.932	0.732	0.295	0.865
	Arterial Tube-Load Model	0.994	0.943	0.997	0.891	0.962	0.986	0.987	0.981	0.963	0.943	0.888	0.802	0.945***

RMSE is root-mean-squared-error; *: $p<0.02$; **: $p<0.05$; ***: $p<0.1$

Table 3 Subject-by-Subject Results for Sequential Central and Peripheral BP Waveforms from Dogs.

RMSE [mmHg]	Dog	1	2	3	4	5	6	Averag
Diastolic BP	Foot-to-Foot Detection	5.3	3.5	4.9	5.9	8.5	12.0	6.7
	Arterial Tube-Load Model	4.9	2.7	2.2	5.4	4.2	6.8	4.4**
Mean BP	Foot-to-Foot Detection	5.6	4.7	5.3	4.0	8.7	14.1	7.1
	Arterial Tube-Load Model	4.2	4.2	1.8	4.0	10.1	7.5	5.3
Correlation [unitless]	Dog	1	2	3	4	5	6	Averag
Diastolic BP	Foot-to-Foot Detection	0.983	0.877	0.968	0.438	0.903	0.897	0.844
	Arterial Tube-Load Model	0.986	0.926	0.994	0.57	0.977	0.968	0.903
Mean BP	Foot-to-Foot Detection	0.988	0.911	0.977	0.842	0.948	0.900	0.928
	Arterial Tube-Load Model	0.993	0.931	0.997	0.836	0.928	0.972	0.943

Table 4 Subject-by-Subject Results for Simultaneous Central BV and Peripheral BP Waveforms from Swine.

RMSE [mmHg]	Pig	1	2	3	4	5	Average
Diastolic BP	Foot-to-Foot Detection	9.2	13	10.3	10.5	13.1	12.2
	Arterial Tube-Load Model	7.7	6.5	4.5	10.3	6.0	7.0*
Mean BP	Foot-to-Foot Detection	11.1	14.5	11.9	18.9	12.2	13.7
	Arterial Tube-Load Model	9.8	7.1	6.1	13.4	8.8	9.0*
Correlation [unitless]	Pig	1	2	3	4	5	Average
Diastolic BP	Foot-to-Foot Detection	0.777	0.687	0.521	0.311	0.588	0.577
	Arterial Tube-Load Model	0.853	0.931	0.927	0.774	0.928	0.883*
Mean BP	Foot-to-Foot Detection	0.8	0.732	0.647	0.306	0.761	0.649
	Arterial Tube-Load Model	0.845	0.944	0.921	0.738	0.883	0.866**

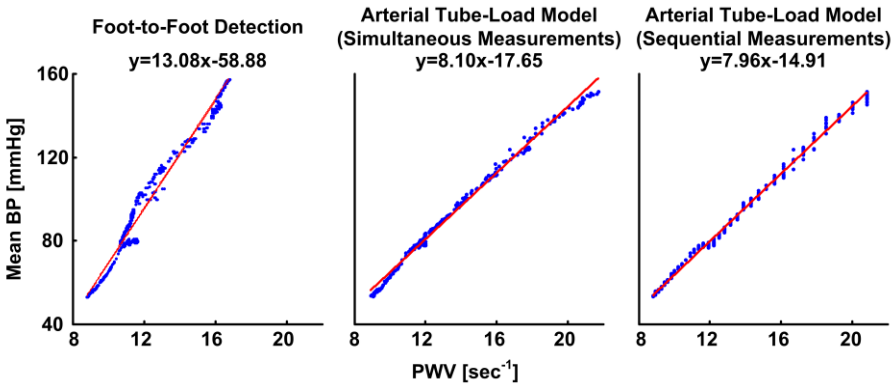

Figure 2-4 Sample plots of mean BP versus PWV estimates from simultaneously and sequentially measured central and peripheral BP waveforms from Dog 3.

A value of unity was used here and elsewhere for the length component of the PWV estimates, as it has no impact on the correlation between BP and PWV within a subject. Red line and equation indicates line of best fit. (Note that the PWV estimates are clustered for the sequential measurements due to waveform sampling and that this clustering is masked for the simultaneous measurements due to averaging the PWV estimates.)

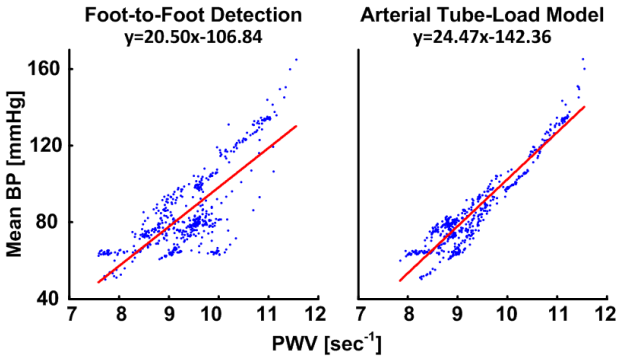

Figure 2-5 Sample plots of mean BP versus PWV estimates from simultaneously measured central BV and peripheral BP waveforms from Pig 2.

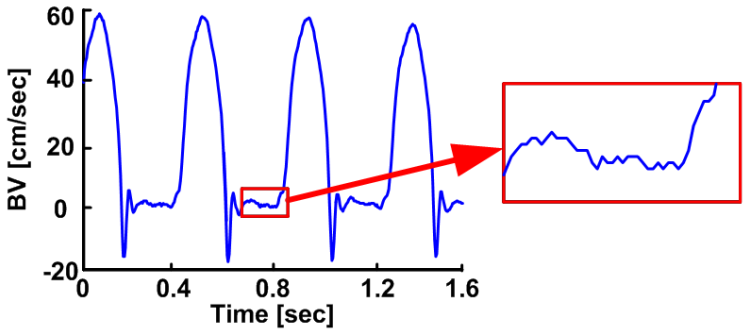

Figure 2-6 Typical noise level in central BV waveform measurement from a pig.

statistically significant only for diastolic BP. Further, the RMSEs and correlation coefficients of the new techniques were not significantly different for simultaneous and sequential measurements (not shown in Tables). For the simultaneous central BV and peripheral BP waveforms from swine, the new technique was able to decrease the average of the RMSEs by 38% and increase the average of the correlation coefficients by 43% relative to the conventional technique. These differences were all statistically significant. Hence, the arterial tube-load model-based paradigm afforded superior improvement in the pigs. The likely reason is that the swine waveforms were contaminated by a greater amount of measurement artifact. That is, these waveforms were measured with an aortic flow probe, which yielded noticeable noise that obfuscated the central BV foot detection as shown in Figure 2-6, and a low fidelity BP catheter, whereas all of the canine waveforms were obtained with high fidelity BP catheters. These results suggest that the new techniques can mitigate waveform artifact.

Finally, the computational speed of the arterial tube-load model-based techniques was about 20% faster than real time when executed in MATLAB on a desktop computer with eight 2.5 GHz processors. In other words, the average PWV estimate over a 15-sec interval of the waveforms could be obtained in about 12 sec on this platform. The speed of the techniques using just one

processor would be about five times slower than real time but may likely be enhanced to at least real time via another programming language.

2.5 Discussion

2.5.1 Summary

We have proposed techniques for improved estimation of PWV, which has emerged as the most important index of arterial stiffness, from central and peripheral BP and/or BV waveforms. The idea is to estimate PWV from the entire waveforms, rather than just their feet, by mathematically eliminating the reflected wave via an arterial tube-load model. Hence, these techniques may be more robust to waveform artifact and more closely indicate the true PWV than the conventional foot-to-foot detection technique. Further, the new techniques are applicable to simultaneously or sequentially measured waveforms and can estimate PWV within or near real-time.

It is not easy to measure the true PWV in absence of wave reflection, so we did not evaluate the techniques against direct reference measurements. However, BP is the major acute determinant of aortic PWV [25], especially under general anesthesia wherein vasomotor tone changes are usually minimal. Hence, we indirectly tested the techniques using BP changes as a reference. We specifically applied the techniques to estimate aortic PWV from simultaneously and sequentially measured central and peripheral BP waveforms and simultaneously measured central BV and peripheral BP waveforms from 17 anesthetized animals during diverse acute interventions that often perturbed BP widely (see Table 1).

Overall, the techniques tracked the BP changes in each subject better than the foot-to-foot-detection technique (see Tables 2-4). This improvement was greater in magnitude in terms of RMSE (about 35% on average) than correlation coefficient (about 20% on average) and reached

statistical significant in most cases. The improvement may have been attained by mitigation of both artifact and wave reflection.

Although the waveforms here were obtained with invasive sensors and thus generally of high quality, the central BV waveforms from the swine still showed a noticeable level of noise (see Figure 2-6). The relative performance of the new techniques was best when applied to these waveforms (see Tables 2-4), thereby indicating their artifact mitigation capability. We expect that these techniques will be able to offer greater improvements in PWV estimation accuracy over the conventional technique when applied to patient waveforms, which are obtained with non-invasive sensors and thus often show much more artifact.

During high rate cardiac pacing, the estimated backward wave was prominent near the central BP waveform foot (see Figure 2-1b). As a result, this apparent foot was at a significantly different location than the "true" foot of the estimated forward wave (see Figure 2-1b), thereby suggesting wave reflection interference mitigation capability of the new techniques.

2.5.2 Extension of Techniques for Local PWV Estimation

According to the Waterhammer equation [13], PWV is also sometimes determined as the characteristic impedance times the arterial area divided by the blood density. The numerator term is estimated by measuring central BP and BV waveforms and then finding the slope of the line that best relates the initial systolic samples of the waveforms [46]. This technique estimates local PWV unlike the foot-to-foot detection technique, which estimates regional PWV. However, the early systolic BV-BP slope technique can similarly be compromised by wave reflection interference and waveform artifact.

The arterial tube-load model-based techniques were designed to obtain an artifact robust estimate of the true regional PWV from central and peripheral BP and/or BV waveforms. However, they can potentially be extended to likewise yield an artifact robust estimate of the true local PWV from central BV and BP waveforms as follows.The arterial tree is modeled as a single uniform tube with terminal load, as shown in Figure 2-7a. The tube represents the wave travel path along a segment of the aorta and likewise has constant characteristic impedance

$$Z_{c0} = \sqrt{\frac{\rho L_0}{A_0 C_0}} \tag{2.4}$$

where L_0, A_0, and C_0 are aortic segment length, area, and compliance and allows waves to travel with constant PTT

$$T_{d0} = \sqrt{\frac{\rho L_0 C_0}{A_0}} \tag{2.5}$$

The load represents the remainder of the arterial tree and similarly has frequency-dependent impedance $[Z_0(\omega)]$ characterized by the total peripheral resistance $[r_0]$ and compliance $[c_0]$ and Z_{c0}. According to this model, the transfer function relating a central BV waveform $[u_c(t)]$ to a central BP waveform $[p_c(t)]$ may be defined in terms of T_{d0}, r_0c_0, $Z_{c0}c_0$, and A_0Z_{c0}, as shown in Figure 2-7b. These four parameters are estimated analogously to the regional PWV estimation techniques. Local PWV is then computed from the A_0Z_{c0} estimate and the nominal ρ value, as shown in Figure 2-7c.

However, this extended technique obviously needs to be tested. Note that it may likewise be amenable to sequential waveform measurements (see Figure 2-3).

2.5.3 Relationship to Previous Techniques

Related techniques have been proposed in the literature. We compare and contrast the arterial tube-load model-based techniques here with several previous techniques.

Techniques have been proposed to estimate regional PWV from central and peripheral waveforms using a black-box, rather than physical model-based, transfer function [47][48]. In particular, an impulse response is identified that optimally couples the central waveform to the peripheral waveform. Then, PTT is determined as the time delay of the impulse response. Hence, these techniques may likewise be robust to artifact and reveal the true PWV. A significant advantage of the techniques is that they are applicable to arbitrary waveforms (e.g., pulse oximeter and impedance waveforms) rather than being limited to BP and BV waveforms. On the other hand, the arterial tube-load model-based techniques here extract PTT not just from the time delay of the transfer function but also from its shape (see T_{di} parameter in the transfer functions of Figure 2-2b) and could thus be more accurate.

Arterial tube-load model-based techniques have been proposed to estimate regional PWV from only peripheral BP waveforms. One technique models multiple peripheral BP waveforms as outputs to the common central BP waveform input [33]. The transfer functions that couple the common input to each output is defined in terms of the parameters of an arterial tube-load model. These parameters, which represent PTT to each peripheral artery and other arterial properties, are then estimated from two or more peripheral BP waveforms via multi-channel blind system identification. Another technique defines the transfer function relating a peripheral BP waveform to the central BP waveform in terms of the arterial tube-load model parameters (see Figure 2-2a) [36]. PTT and the other model parameters are then estimated from one peripheral BP waveform and a one-time PTT measurement by exploiting the fact that central BV is

negligible during diastole. A third technique uses the same model-based transfer function and estimates its parameters from one peripheral BP waveform by assuming that the central BP waveform obeys certain smoothness constraints [34]. These techniques have reduced measurement requirements and are thus more convenient than the techniques here as well as the conventional techniques. However, for the same reason, the previous techniques should yield markedly less accurate PWV estimates. For example, the PTT estimates even from multiple peripheral BP waveforms are unable to indicate the absolute PTT value [34].

Finally, an arterial tube-load model-based technique has been proposed to estimate forward and backward waves from central and peripheral BP waveforms [35]. In particular, the PTT model parameter is first estimated via the foot-to-foot detection technique. Then, with PTT known, both the order and parameters of the load are estimated in closed-form. While this technique is similar to the techniques here, it obviously does not offer an improved PWV estimate.

2.5.4 Contributions

As just indicated, the unique idea here is to enhance PWV estimation accuracy by combining the arterial tube-load model with standard measurements that are being made in practice. Some other contributions of this study are: (a) defining an ECG gating approach to be able to apply arterial tube-load model-based PWV estimation techniques to sequential measurements; (b) developing ways to augment the speed of these techniques; (c) demonstrating that the techniques can indeed improve the accuracy of regional PWV estimates from BP and/or BV waveforms and simultaneous or sequential measurements; and (d) proposing to improve the estimation of local PWV from standard measurements via an arterial tube-load model-based technique.

2.5.5 Limitations

Some limitations of this study are as follows. Firstly, the arterial tube-load model employed here (see Figure.2-2 and 2-7) ignores elastic and geometric tapering and, to a large extent, branching [49]. The model thus assumes that the main reflection sites are at the small arteries. While other reflection sites may also be important in actuality [50][51], the arterioles may indeed often constitute the dominant wave reflection site [52]. One reason is that this site is where the arterial radius changes most abruptly [49]. As a result, the model is usually able to predict experimental BP and BV waveforms quite well [49]. Further, this simplicity affords a small number of parameters that can be uniquely estimated, but with some bias, from limited measurements. Note that the foot-to-foot detection technique may likewise be subject to similar assumptions. Secondly, while the arterial tube-load model-based techniques for regional PWV estimation (see Figure 2-2) may offer a means to improve the accuracy of PTT, they do not address the distance between the measurement sites that is also needed to compute PWV. Hence, the distance measurement component of regional PWV estimation remains problematic [53]. Note that this component is important for comparisons amongst patients but has little value in tracking arterial stiffness changes within a patient. Finally, BP is surely not an ideal reference for assessing the aortic PWV estimates in general. However, the acute BP changes likely sufficed as a reference in this study because vasomotor tone generally has little impact on the large, elastic arteries [25], especially under general anesthesia, and other mechanisms for arterial compliance changes occur very slowly over time (e.g., aging, disease). If BP were a poor reference here, it is unlikely that the new techniques would consistently track the BP changes better than the conventional technique.

2.6 Conclusions

In sum, we have proposed and evaluated arterial tube-load model-based techniques for estimating PWV from a pair of hemodynamic waveforms. Our results indicate that these techniques (a) can improve PWV estimation accuracy by mitigating waveform artifact and wave reflection interference and (b) are applicable to simultaneously or sequentially measured central and peripheral BP and/or BV waveforms.

Future efforts are needed to bring these techniques to practice. Most importantly, since humans may show different wave reflection patterns than animals, human testing is mandatory. For example, the techniques should be evaluated in patients in terms of both accuracy and predictive value relative to the conventional techniques. It would also be worthwhile to refine the new techniques, especially by exploring more accurate arterial models. If subsequent studies prove successful, then these techniques may be employed for more faithful monitoring of arterial stiffness in hypertensive, end-stage renal disease, diabetic, and geriatric patients. A more immediate application could be to use the techniques as a short-term surrogate outcome of clinical trials for determining the efficacy of therapies aimed at reducing arterial stiffness.

Chapter 3. Estimation of Pulse Transit Time as a Function of Blood Pressure Using a Nonlinear Arterial Tube-Load Model

3.1 Introduction

Pulse transit time (PTT) is the time delay for the pressure wave to travel between proximal and distal arterial sites. According to the Bramwell-Hill equation, PTT varies with the arterial compliance. Since arterial compliance decreases as blood pressure (BP) increases, PTT is also often inversely correlated to BP. PTT can be estimated simply via the relative timing between proximal and distal waveforms reflecting the arterial pulse. Hence, PTT has proven to be a convenient marker of arterial stiffness [54] and could otentially permit cuff-less BP monitoring [55][56][57].

As shown in Figure 3-1(a), the conventional technique for estimating PTT is to detect the trough-to-trough or foot-to-foot time delay between the proximal and distal waveforms [$T_d^{F\text{-}F}$]. The premise is that arterial wave reflection interference is negligible during late diastole and early systole when the waveform feet occur. Hence, by virtue of being estimated at the waveform feet, conventionally estimated PTT is precisely a marker of arterial stiffness at the level of diastolic BP and generally correlates best with diastolic BP [55]. As again shown in Figure 3-1(a), PTT could also be estimated as the time delays between other characteristics points in the waveforms such as the mean level and the peak [$T_d^{M\text{-}M}$ and $T_d^{P\text{-}P}$]. However, because wave reflection interference increases as the cardiac cycle progresses, this naïve technique can yield PTT estimates of little value. For example, as shown in Figure 3-1(b), the peak-to-peak time delay can even be negative.

It would be desirable to have a technique that can reliably estimate PTT as a function of BP (e.g., PTT for each BP level in the cardiac cycle) from proximal and distal waveforms. Such a

technique could be applied to improve arterial stiffness monitoring and help realize cuff-less BP monitoring.

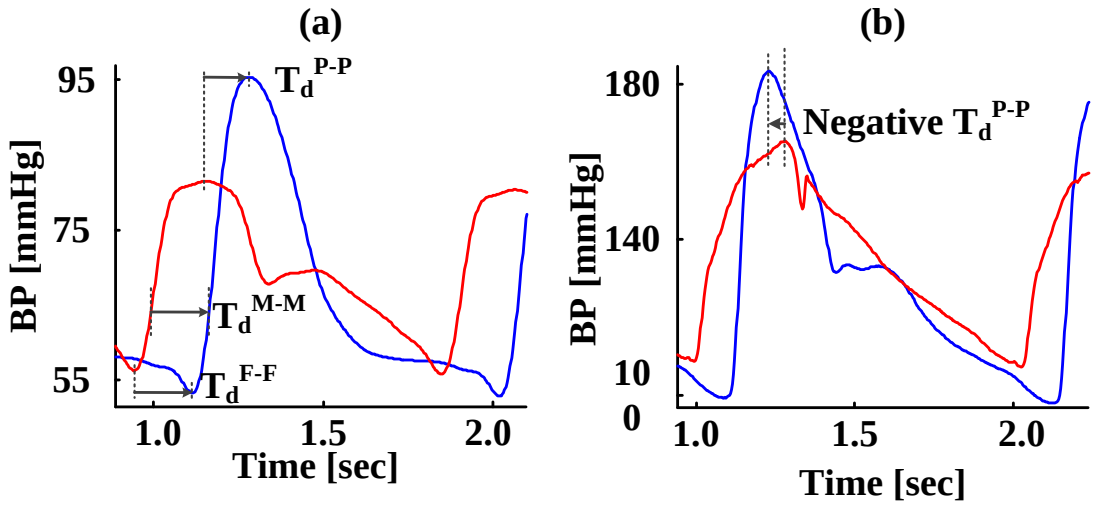

Figure 3-1 Naïve technique for estimation of pulse transit time (PTT) as a function of blood pressure (BP) from proximal (gray) and distal (black) waveforms.
(a) PTT at diastolic, mean, and systolic BP are detected as the foot-to-foot (T_d^{F-F}), mean-to-mean (T_d^{M-M}), and peak-to-peak (T_d^{P-P}) time delays, respectively. (b) The peak-to-peak time delay is often not useful.

For arterial stiffness monitoring, the PTT-BP function estimated by the desired technique could enhance cardiovascular risk stratification over a single PTT estimate at the level of diastolic BP [58][59]. In addition, the technique could be used to correct PTT for BP and thereby afford more meaningful tracking of arterial stiffness in an individual patient over time or more meaningful comparisons of arterial stiffness amongst different patients.

For cuff-less BP monitoring, the desired technique could be used to calibrate PTT (in units of msec) to BP (in units of mmHg). The conventional approach for constructing a patient-specific curve that relates PTT to BP (i.e., PTT as a function of BP) involves measuring pairs of PTT and BP values in a patient during an experimental perturbation that varies PTT and BP over a

significant range. (BP could thereafter be measured in that patient without using a cuff by applying the calibration curve to PTT.) However, the experimental perturbation makes this approach less practical. The desired technique could provide the requisite curve without the need for inducing an artificial BP change (i.e., a "perturbation-less calibration" approach).

In this paper, we propose a technique for estimating PTT as a function of BP from proximal and distal BP waveforms using a nonlinear arterial tube-load model. The model accounts for the BP-dependent arterial compliance and peripheral wave reflection. In this way, PTT may be effectively estimated at the multiple BP levels in the cardiac cycle after mathematically eliminating the reflected wave. We demonstrate the efficacy of this technique in terms of calibration of PTT to BP in animals subjected to hemodynamic interventions, which perturbed BP over a wide range, and correlation between the multiple PTT estimates and corresponding BP levels in patients receiving sublingual nitroglycerin, which altered systolic BP but not diastolic BP. A preliminary version of this manuscript has been reported in abbreviated form [60].

3.2 Methods

The technique proposed herein represents an extension of a previous technique that we introduced to robustly estimate PTT from proximal and distal BP waveforms using a linear arterial tube-load model [61]. We first review this linear arterial tube-load model technique for estimating a single PTT value. We then present the extended nonlinear arterial tube-load model technique for estimating PTT as a function of BP from the same waveforms. We thereafter describe the experimental data and data analysis that we employed to demonstrate the value of the proposed technique.

3.2.1 Linear Arterial Tube-Load Model Technique for Robust Estimation of PTT

This technique is illustrated in Figure 3-2 and described in detail elsewhere [61]. The underlying linear model assumes that arterial compliance is constant (for each segment of waveforms for analysis) but accounts for peripheral wave reflection. In this way, the true PTT may be robustly estimated from the entire waveforms, rather than just their feet, after mathematically eliminating the reflected wave.

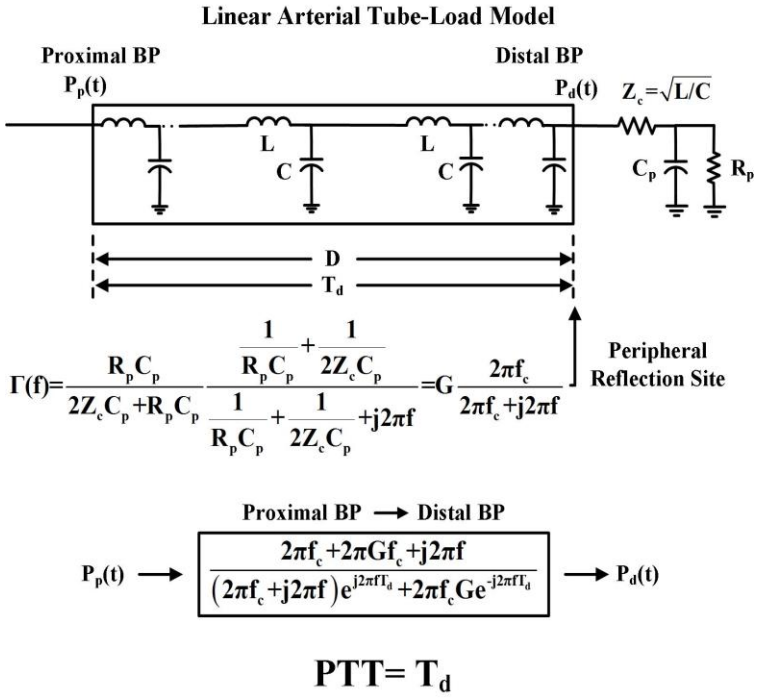

Figure 3-2 Previous linear arterial tube-load model technique for robust estimation of PTT from proximal and distal BP waveforms [$P_p(t)$ and $P_d(t)$].
The linear model accounts for peripheral wave reflection but assumes constant arterial compliance (top panel). The parameters [T_d (PTT), G (gain of reflection coefficient $\Gamma(f)$), f_c ($\Gamma(f)$ cutoff frequency)] are estimated by finding the transfer function that optimally fits $P_p(t)$ to $P_d(t)$ (middle panel). PTT is then given as the T_d estimate (bottom panel).

More specifically, the relationship between the measured proximal and distal BP waveforms is modeled with a linear, elastic tube terminated by a lumped parameter load (see top panel of

Figure 3-2). The tube represents the large artery path for the pressure wave to travel between the two measurement sites. This tube is assumed to be uniform and frictionless [61]. Hence, it is mathematically equivalent to an ideal, lossless transmission line (which is the form of the model shown in Figure 3-2) and has constant characteristic impedance [$Z_c=\sqrt{L/C}$, where L and C are the constant large artery inertance and compliance per unit length] and allows pressure waves to travel with constant PTT between the tube ends [$T_d=D\sqrt{L/C}$, where D is the length of the tube]. The load represents the major small artery site for wave reflection [49]. This load is characterized by peripheral resistance and compliance [R_p and C_p] while matching the tube impedance at infinite frequency.

Waves traveling along the tube in the forward direction (left-to-right) are reflected in the backward direction at the load with a frequency-dependent reflection coefficient [$\Gamma(f)=G\frac{2\pi f_c}{2\pi f_c+2\pi f}$, where $G=\frac{R_pC_p}{2Z_cC_p+R_pC_p}$ and $f_c=\frac{1}{R_pC_p}+\frac{1}{2Z_cC_p}$] in order to mimic arterial wave transmission and peripheral wave reflection. According to the model, a transfer function defined by three unknown parameters [T_d, G, f_c] relates proximal BP [$P_p(t)$] to distal BP [$P_d(t)$] (see middle panel of Figure 3-2). The parameters are estimated by finding the transfer function, which when applied to $P_p(t)$, best fits $P_d(t)$ in the least squares sense. This optimization is achieved via an exhaustive search over a justifiable range of the parameters. This range is specifically as follows: T_d = [$0.5\cdot T_d^{F\text{-}F}$:2:$1.5\cdot T_d^{F\text{-}F}$] msec; G = [0:0.025:1] unitless, which constitutes the physical range of G; and f_c = [0:0.1:15] Hz, which covers the typical frequency range of BP waveforms. PTT is finally given as the T_d estimate (see bottom panel of Figure 3-2). This estimate may be most indicative of PTT at the level of mean BP, as it is determined from the entire waveforms.

3.2.2 Nonlinear Arterial Tube-Load Model Technique for Estimation of PTT as a Function of BP

This technique is illustrated in Figure 3-3. The technique extends the linear arterial tube-load model technique by making the arterial compliance dependent on BP instead of being constant. The resulting nonlinear arterial tube-load model may thus permit estimation of PTT as a function of BP after mathematically eliminating the reflected wave.

More specifically, the large artery compliance per unit length in the model is dependent on BP according to the following experimentally derived relationship: $C_0e^{-\alpha P}$, where P is BP, C_0 is the compliance per unit length at zero BP, and $\alpha > 0$ indicates the extent of the BP dependency on the compliance [21] (see top panel of Figure 3-3). As outlined in [55][62], PTT and BP in the resulting nonlinear, lossless transmission line model are related as follows:

$$PTT=\sqrt{D^2LC_0e^{-\alpha P}}\,. \tag{3.1}$$

Hence, the model parameters specify the function relating BP to PTT. All unknown parameters are estimated from the proximal and distal BP waveforms as follows.

Since the model is nonlinear, it cannot represent the relationship between the proximal and distal BP waveforms with a transfer function. A finite difference method is thus used to relate the waveforms (see Appendix) [63]. The resulting numerical relationship is defined by four unknown parameters [D^2LC_0, α, G, f_c]. This number of parameters may be reduced by one. In particular, the linear arterial tube-load model technique is first applied to the measured waveforms to estimate PTT = T_d, and mean BP is determined. This pair of values is then substituted into Eq. (3.1) to constrain D^2LC_0 entirely by the value of α. Hence, three unknown parameters [α, G, f_c] remain for estimation (see middle panel of Figure 3-3). These parameters

are estimated by finding the finite difference relationship, which when applied to $P_p(t)$, best fits $P_d(t)$ in the least squares sense. This optimization is likewise achieved via an exhaustive search over a wide range of the parameters. This range is specifically as follows: α = [0:0.001:0.05] $mmHg^{-1}$, which generously encompasses the nominal α value of 0.016-0.018 $mmHg^{-1}$ [21]; G = [0:0.025:1] unitless; and f_c = [0:0.1:15] Hz. PTT as a function of BP is finally given as Eq. (3.1) equipped with the α and D^2LC_0 estimates (see bottom panel of Figure 3-3).

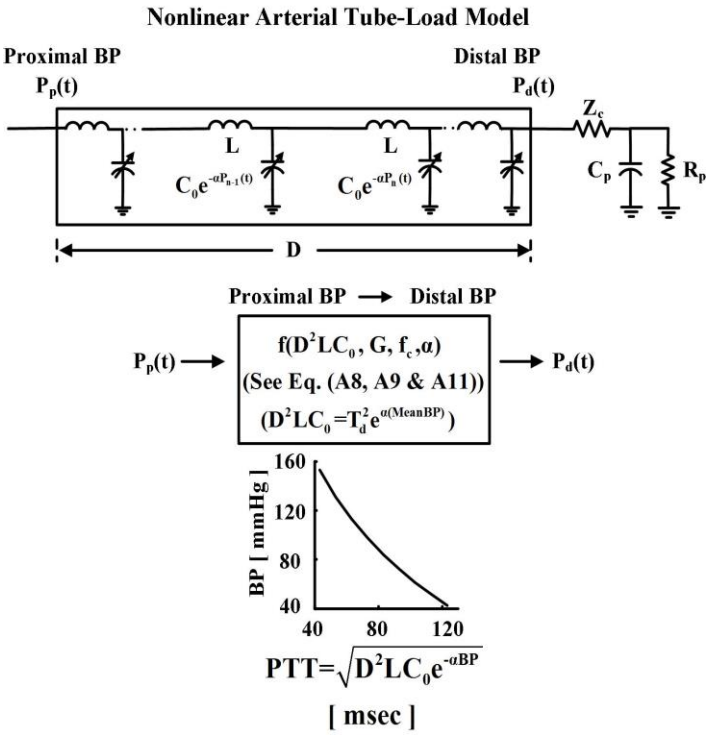

Figure 3-3 Proposed nonlinear arterial tube-load model technique for estimation of PTT as a function of BP from proximal and distal BP waveforms.
The nonlinear model accounts for BP-dependent arterial compliance and peripheral wave reflection (top panel). The parameters [α (degree of BP-dependence), G, f_c] are estimated by finding the finite difference relationship (see Appendix) that optimally fits $P_p(t)$ to $P_d(t)$ (middle panel). PTT as a function of BP is then given via the α estimate and D^2LC_0, which is specified by the T_d estimate via the linear arterial tube-load model technique and mean BP (bottom panel).

3.3 Experimental Data

We assessed the proposed technique using animal and patient data that we previously collected. These data are described in detail elsewhere [61][64]. We mention the most relevant aspects of the data below.

The animal data were obtained under protocols approved by the Michigan State University All-University Committee on Animal Use and Care [61]. These data included invasive aortic and femoral artery BP waveforms sampled at 500 Hz from 12 healthy adult beagles (10-12 kg) during a baseline period and two to four hemodynamic interventions (amongst low and high rate cardiac pacing, dobutamine, esmolol, verapamil, phenylephrine, vasopressin, nitroglycerin, norepinephrine, xylazine, saline, hemorrhage). Table 1 shows the group average (mean±SE) range of diastolic, mean, and systolic BP and the group average correlation coefficients between pairs of the BP levels. Hence, all BP levels varied widely, but similarly, in each subject.

The patient data were obtained under a protocol approved by the Taipei Veterans General Hospital Institutional Review Board [64]. These data were de-identified and included invasive aortic and brachial artery BP waveforms sampled at 500 Hz from 54 cardiac catheterization patients (66±13 years; 81% male; clinical diagnoses of mainly hypertension (59% of patients), coronary artery disease (59%), dyslipidemia (31%), and/or diabetes (22%)) before and after sublingual nitroglycerin administration. Table 1 also shows the group average of diastolic, mean, and systolic BP during the baseline period and nitroglycerin administration. Hence, systolic BP, but not diastolic BP, was altered by the intervention.

Table 5 Group average (mean±SE) blood pressure (BP) statistics

Animal Data	BP Range [mmHg]		
	Diastolic BP	Mean BP	Systolic BP
Minimum	39±2	52±2	72±4
Maximum	99±8	125±9	173±11
	Correlation Coefficient		
	Diastolic BP vs. Mean BP	Diastolic BP vs. Systolic BP	Mean BP vs. Systolic BP
	0.96±0.02	0.84±0.06	0.94±0.02
Patient Data	BP Level [mmHg]		
	Diastolic BP	Mean BP	Systolic BP
Baseline	70±1	97±2	141±2
Nitroglycerin	69±2	88±2	124±2

3.4 Data Analysis

We analyzed the experimental data to assess the proposed technique in three ways. Details follow.

First, we assessed the proposed technique in terms of its ability to improve the fit of the distal BP waveform over the linear arterial tube-load model technique. We used both the animal and patient data for this assessment. We computed the root-mean-square-error (RMSE) between the estimated and measured distal BP waveforms for both techniques. We also computed the same RMSE value for the linear arterial tube-load model technique, as implemented with a finite difference method instead of the transfer function, to determine the impact of using the numerical method. We then compared the RMSE values of the techniques using paired t-tests. A $p < 0.0167$ (= 0.05/3) was considered significant based on Bonferroni correction for the three pairwise comparisons.

Second, we assessed the proposed technique in terms of its ability to calibrate PTT to BP. We used the baseline period data to construct the calibration curve and the hemodynamic intervention data to test the curve. We employed the animal data here, because the hemodynamic interventions varied BP enough to offer a meaningful assessment (see Table 1). More specifically, we applied the technique to the proximal and distal BP waveforms from the baseline period of each subject to estimate PTT as a function of BP and thereby create subject-specific calibration curves. We then applied the linear arterial tube-load model technique to 15-sec segments of the proximal and distal BP waveforms from the hemodynamic interventions. We next applied the resulting PTT values for a subject to the calibration curve for that subject to estimate mean BP during the interventions. We finally computed the bias error (μ) and precision error (σ) between the estimated and measured mean BP. Note that the nonlinear arterial tube-load model technique can yield a nearly constant PTT when, for example, pulse pressure is small or elastin dominates arterial wall mechanics such that the arterial pressure-volume relationship is linear [55]. In this case, the estimated PTT-BP function would not be useful for calibration. Hence, if the technique does not significantly reduce the RMSE between the estimated and measured distal BP waveform relative to the linear arterial tube-load model technique for a given subject, then a calibration curve will not be outputted for that subject.

Third, we assessed the proposed technique in terms of its ability to correlate with diastolic, mean, and systolic BP. We employed the patient data here, because sublingual nitroglycerin changed the BP levels differently enough to offer an interesting assessment (see Table 1). We applied the technique to the proximal and distal BP waveforms to estimate PTT as a function of BP. We then substituted the measured diastolic, mean, and systolic BP into this function to estimate PTT at the three BP levels. We next compared the changes in these PTT estimates induced by the

intervention to the corresponding changes in the measured BP levels, again using paired t-tests and a significance level of $p < 0.0167$. For comparison, we likewise assessed the PTT estimates of the naïve technique of Figure 3-1(a).

3.5 Results

Figure 3-4 shows the group average (mean±SE) of the RMSE between the distal BP waveforms measured and estimated by the nonlinear and linear arterial tube-load model techniques for the animals during the baseline period and patients. Figure 3-5 shows representative examples of the measured and estimated distal BP waveforms. The RMSE values were similar for the animals and patients. Overall, the proposed technique reduced the RMSE by 24% and 35% compared to the linear arterial tube-load model technique, as implemented with a transfer function and finite difference method, respectively. These reductions were statistically significant. Hence, the proposed technique, which fits the distal BP waveform using the same number of parameters as the linear arterial tube-load model technique, was able to improve the fitting despite the numerical error introduced by the finite difference method.

Figure 3-6 shows the calibration curves derived by the nonlinear arterial tube-load model technique for each animal during the baseline period. This figure also includes pairs of PTT estimated by the linear arterial tube-load model technique and measured mean BP during the hemodynamic interventions (i.e., data not seen by the calibration curve). In one subject, the RMSE between the estimated and measured distal BP waveform was only 2% smaller than that obtained by the linear arterial tube-load model technique as implemented with the finite difference method. Hence, the proposed technique did not output a calibration curve for this subject. Note that this technique achieved an RMSE reduction of at least 30% in every other subject and thereby produced testable calibration curve in these subjects. As expected, the

correspondence between the calibration curve and the PTT-mean BP pairs was generally best for the BP range used to generate the curve (indicated with vertical arrows). Table 2 shows the bias and precision errors between the mean BP estimated by applying the PTT estimates from the linear arterial tube-load model technique to the calibration curve and the measured mean BP for each subject during the hemodynamic interventions. The group average bias and precision errors were 5.1±3.0 and 6.6±3.5 mmHg, respectively. Hence, the proposed technique was able to generate useful calibration curves. Note that the naïve technique of Figure 3-1 (a) could also be applied to generate a calibration curve from the baseline proximal and distal BP waveforms by, for example, fitting a line through its three PTT estimates and the corresponding BP levels.

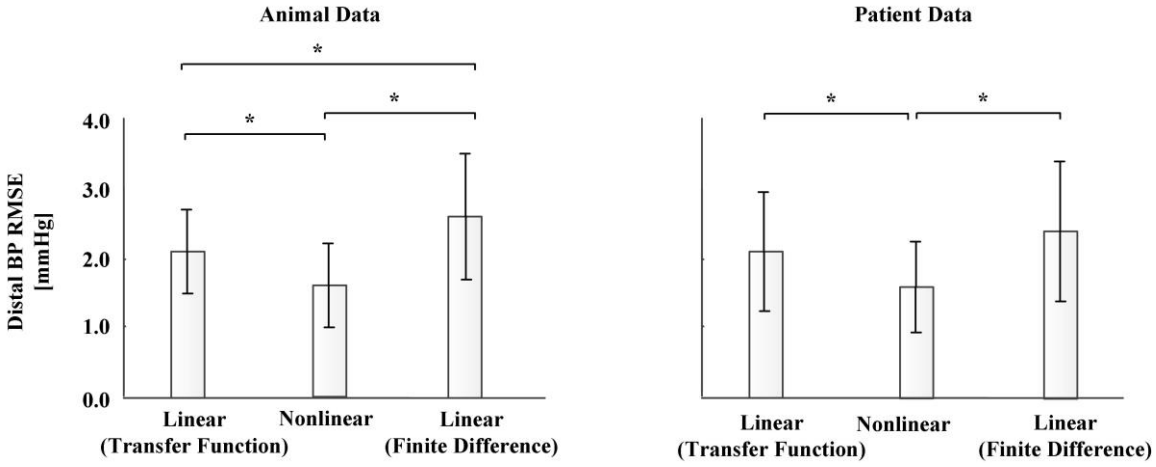

Figure 3-4 Group average (mean±SE) of the root-mean-squared-error (RMSE) between the distal BP waveofmrs measured and estimated by the nonlinear and linear arterial tube-load model techniques. * indicates statistical significance.

However, these calibration curves produced inaccurate mean BP estimates during the interventions that were not worth showing. Hence, the naïve technique was not able to provide any competition to the proposed technique in terms of calibrating PTT to BP.

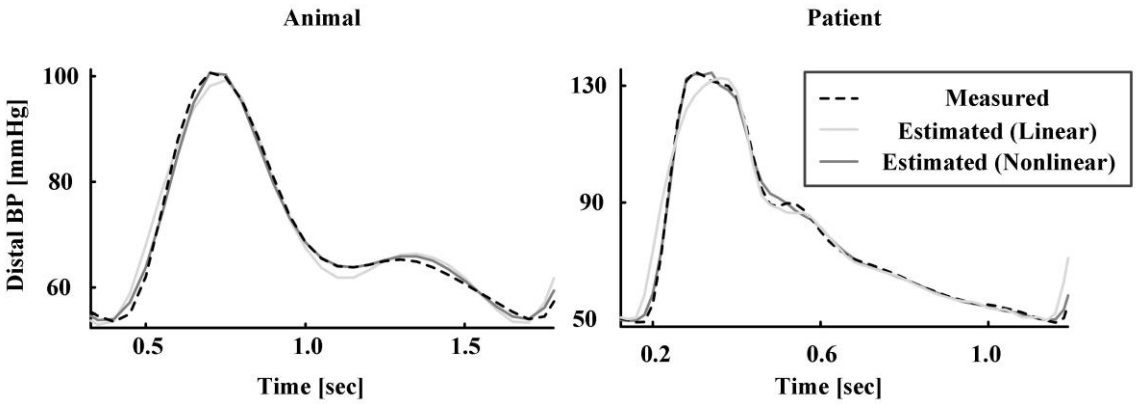

Figure 3-5 Examples of distal BP waveforms measured and estimated by the nonlinear and linear arterial tube-load model techniques

Figure 3-7 (a) shows the group average of the changes in diastolic, mean, and systolic BP induced by sublingual nitroglycerin administration in the patients. Systolic BP decreased the most, followed by mean BP, and then diastolic BP. These differences were statistically significant. Figure 3-7(b) shows the group average of the nitroglycerin-induced changes in PTT at the levels of diastolic, mean, and systolic BP estimated by the nonlinear arterial tube-load model technique. PTT at the level of systolic BP increased the most, followed by PTT at the level of mean BP, and then PTT at the level of diastolic BP. These differences were likewise statistically significant. Hence, the proposed technique was able to correlate with the three differently varying BP levels on average. Figure 3-7(c) shows the group average of the corresponding PTT changes estimated by the naïve technique of Figure 3-1(a). The change in PTT at the level of systolic BP [$T_d^{P\text{-}P}$] was not significantly different from the changes in PTT at the other two BP levels [$T_d^{F\text{-}F}$ and $T_d^{M\text{-}M}$]. Hence, the naïve technique was not able to correlate with the BP levels as well as the proposed technique.

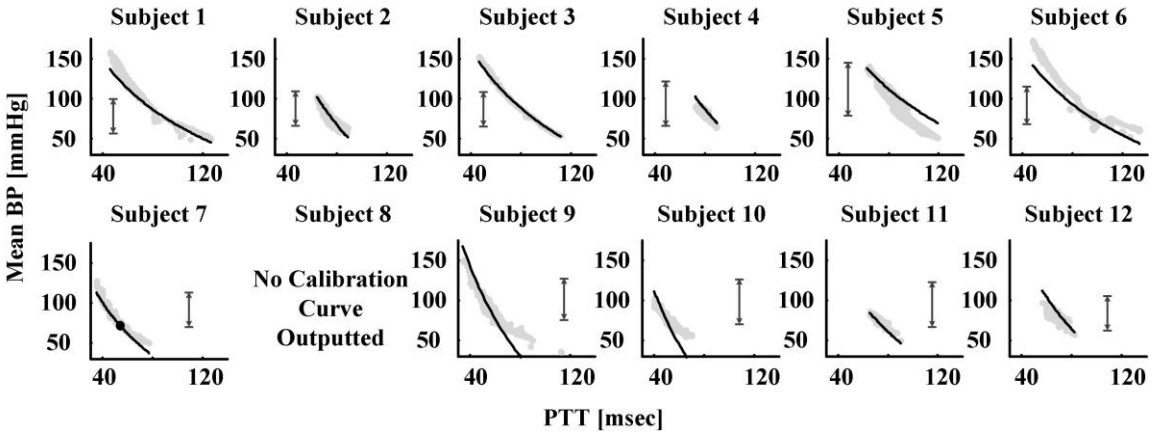

Figure 3-6 Calibration curves (black lines) derived by the nonlinear arterial tube-load model technique during the baseline period along with pairs of PTT estimated by the linear arterial tube-load model technique and measured mean BP (gray dots) during the hemodynamic interventions.

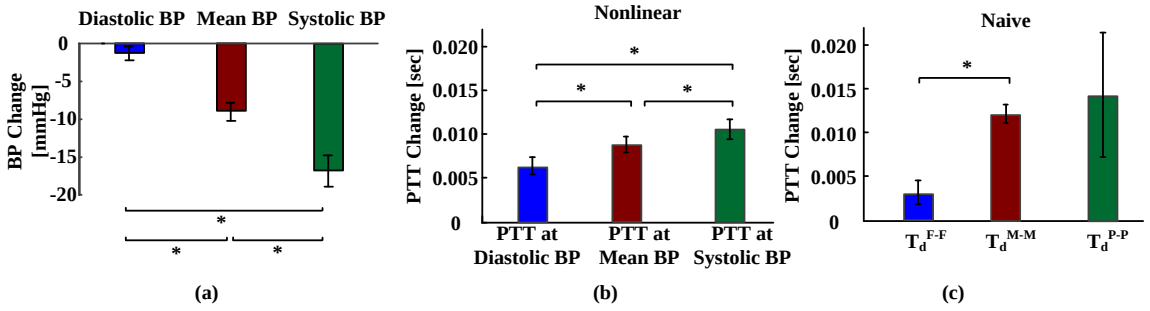

Figure 3-7 Group average of the nitroglycerin-induced BP changes and corresponding PTT changes estimated by the nonlinear arterial tube-load model and naïve (see Figure 3-1) techniques in patients.

3.6 Discussion

PTT varies with BP throughout the cardiac cycle, yet, because of wave reflection, only one PTT value at the level of diastolic BP is conventionally estimated from proximal and distal arterial waveforms (see Figure 3-1). We developed a technique to estimate PTT as a function of BP from proximal and distal BP waveforms using a nonlinear arterial tube-load model (see Figure 3-3). This model accounts for the BP-dependent arterial compliance (which makes it nonlinear) and the main wave reflection site at the periphery. Through finite differencing (see Appendix),

the model provides a relationship from the proximal BP waveform to the distal BP waveform in terms of four unknown parameters. One parameter is effectively estimated by first applying a linear arterial tube-load model technique to the waveforms (see Figure 3-2). The remaining three parameters are then estimated so as to optimally couple or fit the proximal BP waveform to the distal BP waveform through the finite difference relationship. PTT as a function of BP is finally specified by the parameter estimates. In this way, multiple PTT values corresponding to each BP level in the cardiac cycle may be estimated after mathematically eliminating the reflected wave.

The proposed nonlinear arterial tube-load model technique could potentially be applied to improve arterial stiffness monitoring and help realize cuff-less BP monitoring. For the former application, the technique may offer a marker of arterial stiffness at both diastolic and systolic BP levels, which could enhance cardiovascular risk stratification [58][59] and permit correction of PTT estimates for the BP level. For the latter application, the technique may afford a patient-specific curve to calibrate PTT to BP by exploiting the natural pulsatile variation in BP rather than employing an inconvenient and possibly unsafe experimental perturbation to vary BP.

We tested the proposed technique in terms of its ability to fit the distal BP waveform, calibrate PTT to BP, and correlate with multiple BP levels using data from 12 animals whose BP levels varied widely but similarly and 54 cardiac catheterization patients whose BP levels varied differently but to a much lesser extent (see Table 1). For comparison, we likewise tested competing techniques including the naïve technique of Figure 3-1(a), which ignores wave reflection to estimate multiple PTT values via time delays at various BP levels.

The proposed technique fitted the distal BP waveforms well for both the animal and patient data (see Figure 3-5). Further, it often provided better fitting than the linear arterial tube-load model

technique in which the underlying model assumes that the arterial compliance is constant but is otherwise similar (see Figure 3-4). Note that the superior fitting was achieved despite using the same number of parameters for the fit and numerically implementing the nonlinear model.

The proposed technique generated subject-specific calibration curves from the baseline period of the animal data that corresponded reasonably well to the pairs of mean BP and PTT estimates of the linear arterial tube-load model technique from the hemodynamic intervention periods (see Figure 3-6). The bias and precision errors of the "cuff-less" mean BP measured by applying these PTT estimates to the calibration curves during the hemodynamic interventions were near the AAMI accuracy limits (see Table 2). However, the proposed technique may not always generate a calibration curve. In particular, if the technique does not significantly reduce the distal BP waveform fitting error compared to the linear arterial tube-load model technique, then PTT may be nearly constant. In this case, which can occur when the pulse pressure and/or mean BP are small [55], a useful calibration curve would not be obtained. The proposed technique did not output a calibration curve for one of the 12 animals in this study. Note that the naïve technique did not provide reasonable calibration curves for most of the subjects (results not worth showing).

The proposed technique produced PTT estimates at the levels of diastolic, mean, and systolic BP that, on average, tracked the different diastolic, mean, and systolic BP changes induced by the hemodynamic intervention in the patient data (see Figure 3-7 (a)&(b)). By contrast, the naïve technique could not track the systolic BP changes well via the peak-to-peak time delay or otherwise (see Figure 3-7(c)).

We used invasive BP waveforms in this study to demonstrate the potential of the nonlinear arterial tube-load model technique. In practice, the technique could be applied to non-invasive carotid and femoral BP waveforms via applanation tonometry. These waveforms are commonly measured to obtain conventional PTT estimates for arterial stiffness monitoring [54]. Hence, the technique could be applied to waveforms that are already being measured to offer more information about arterial stiffness. In addition, after applying the technique to derive a patient-specific calibration curve from the non-invasive BP waveforms, conventional PTT estimates could be obtained using, for example, photoplethysmography (PPG) waveforms from the neck and upper thigh and then calibrated with the curve to achieve continuous, non-invasive, and cuff-less monitoring of diastolic and mean BP. Note that the calibration curve would have to be determined periodically (e.g., every year) to account for age- and disease-induced changes in PTT. Also note that the computational complexity of the technique, which is not low, may not be a factor for these applications, as the technique would only be applied on occasion and need not produce an estimate in real-time.

3.7 Conclusion

We introduced a technique to estimate PTT as a function of BP from proximal and distal BP waveforms using a nonlinear arterial tube-load model. The model accounts for the BP-dependent arterial compliance and peripheral wave reflection. In this way, PTT may be effectively estimated at the multiple BP levels in the cardiac cycle after mathematically eliminating the reflected wave. Excluding the naïve technique of Figure 3-1(a), we are not aware of any other technique in the literature that is able to estimate PTT values throughout the cardiac cycle from a pair of arterial waveforms. We applied the nonlinear arterial tube-load model technique to invasive BP waveforms from animals and patients and showed that the estimated

PTT-BP function could be used as a subject-specific curve for calibrating PTT to BP and that the estimated PTT at diastolic, mean, and systolic BP levels could correlate with the corresponding BP levels. These results suggest that the technique could potentially be used to help realize cuff-less BP monitoring and improve arterial stiffness monitoring. Future studies of the technique should assess its performance as applied to non-invasive BP waveforms and determine if the estimated PTT-BP function can afford an arterial stiffness marker of clinical value superior to conventional single PTT estimates. In addition, subsequent efforts aiming to extend the technique for estimation of PTT as a function of BP from waveforms that are more easily measured than BP waveforms (e.g., PPG waveforms) may be worthwhile. Such an extended technique would allow for cuff-less monitoring of systolic BP in addition to diastolic BP via PTT.

APPENDIX

APPENDIX

The governing differential equations of the nonlinear arterial tube-load model of Figure 3-3 (top panel) are as follows:

$$-\frac{\partial P(t,x)}{\partial x}=L\frac{\partial \dot{Q}(t,x)}{\partial t} \tag{3.A1}$$

$$-\frac{\partial \dot{Q}(t,x)}{\partial x}=C_0 e^{-\alpha P(t,x)}\frac{\partial P(t,x)}{\partial t} \tag{3.A2}$$

$$\dot{Q}(t,x)=\frac{P(t,x)-\dot{Q}(t,x)Z_c}{R_p}+C_p\frac{d(P(t,x)-\dot{Q}(t,x)Z_c)}{dt} \tag{3.A3}$$

The first two equations govern the transmission line, while the last equation governs the terminal load. P(t,x) and $\dot{Q}(t,x)$ represent BP and blood flow rate as a function of time [t] and space along the line [x]. They are state variables of the model. The input is $P_p(t)$, and the output is $P_d(t)$.

To solve the nonlinear equations, the transmission line was meshed into N nodes for P and N-1 nodes for $\dot{Q}$, as shown in Figure 3-8. The subscript n is the spatial index, while the superscript k is the temporal index. So, P_1^k and P_N^k are $P_p(t)$ and $P_d(t)$, respectively. The distance between adjacent nodes of the same kind is Δx. Eqs. (3.A1)-(3.A3) were discretized using this mesh and Euler's method as follows:

$$\dot{Q}_n^{k+1/2}=\dot{Q}_n^{k-1/2}-\frac{\Delta t}{\Delta x L}(P_{n+1}^k-P_n^k) \qquad \text{for n=1:(N-1)} \tag{3.A4}$$

$$P_{n+1}^k=P_n^k-\frac{\Delta t}{C_0 e^{-\alpha P_n^k}\Delta x}(\dot{Q}_n^{k+1/2}-\dot{Q}_{n-1}^{k+1/2}) \qquad \text{for n=2:(N-1)} \tag{3.A5}$$

$$P_N^{k+1}=(\frac{\Delta t}{Z_c C_p}+\frac{\Delta t}{R_p C_p}+1)Z_c\dot{Q}_{N-1}^{k+1/2}-Z_c\dot{Q}_{N-1}^{k-1/2}+(1-\frac{\Delta t}{R_p C_p})P_N^k \tag{3.A6}$$

The number of unknown parameters in the discretized equations may be reduced as follows. First, since Z_c represents the characteristic impedance of the transmission line, this parameter was defined as follows:

$$Z_c = \sqrt{\frac{L}{C_0 e^{-\alpha \bar{P}}}} \tag{3.A7}$$

where $\bar{P}$ is mean BP. Then, substituting Eq. (3.A7) and $\Delta x = D/(N-1)$ into Eqs. (3.A4)-(3.A6) and applying some simple manipulations gives the following equations:

$$DL\dot{Q}_n^{k+1/2} = DL\dot{Q}_n^{k-1/2} - (N-1)\Delta t(P_{n+1}^k - P_n^k) \qquad \text{for } n=1:(N-1) \tag{3.A8}$$

$$P_{n+1}^k = P_n^k - \frac{(N-1)\Delta t}{D^2 L C_0 e^{-\alpha P_n^k}}(DL\dot{Q}_n^{k+1/2} - DL\dot{Q}_{n-1}^{k+1/2}) \qquad \text{for } n=2:(N-1) \tag{3.A9}$$

$$P_N^{k+1} = \left(\frac{\Delta t}{Z_c C_p} + \frac{\Delta t}{R_p C_p} + 1\right)\sqrt{\frac{1}{D^2 L C_0 e^{-\alpha \bar{P}}}}DL\dot{Q}_{N-1}^{k+1/2} - \sqrt{\frac{1}{D^2 L C_0 e^{-\alpha \bar{P}}}}DL\dot{Q}_{N-1}^{k-1/2} + \left(1 - \frac{\Delta t}{R_p C_p}\right)P_N^k \tag{3.A10}$$

Now, RC and Z_cC may be expressed in terms of G and f_c (see Figure 3-2) so that Eq. (3.A10) becomes the following:

$$P_N^{k+1} = (\Delta t(2\pi f_c + 2\pi f_c G) + 1)\sqrt{\frac{1}{D^2 L C_0 e^{-\alpha \bar{P}}}}DL\dot{Q}_{N-1}^{k+1/2} - \sqrt{\frac{1}{D^2 L C_0 e^{-\alpha \bar{P}}}}DL\dot{Q}_{N-1}^{k-1/2} + (1 - \Delta t(2\pi f_c - 2\pi f_c G))P_N^k \tag{3.A11}$$

The final discretized model equations are Eqs. (3.A8), (3.A9), and (3.A11). Now, the state variables are P and $DL\dot{Q}$, and the unknown parameters are D^2LC_0, α, G, and f_c.

For a given set of parameter values and $P_p(t)$ input, these equations were iteratively solved for $P_d(t)$. The iteration commenced with zero initial conditions. Proportional blood flow rate was

first solved at all nodes using Eq. (3.A8), and then BP was solved at all nodes using Eqs. (3.A9) and (3.A11). This process was repeated for each successive time step.

The values for N and Δt were chosen to balance accuracy and numerical stability. In particular, Δt was set to 0.02 sec, and N was chosen as the largest integer that met the condition: $N \leq 1+\sqrt{D^2 L C_0 e^{-\alpha P_{max}}}/\Delta t$, where P_{max} is the maximal BP that can appear on any node during the numerical simulation. This condition enforces the wave speed to not exceed $\Delta x/\Delta t$ and is required for a stable solution [63].

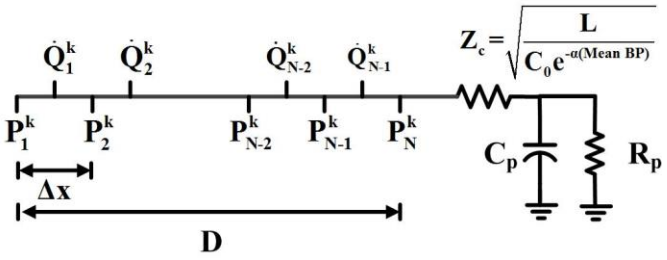

Figure 3-8 Meshing of the nonlinear arterial tube-load model (top panel of Figure 3-3) for numerical solution of the governing model equations.
P is BP, while $\dot{Q}$ is blood flow rate. The superscript k denotes time index, while the subscript N denotes space index.

Chapter 4. Comparison of Non-Invasive Pulse Transit Time Estimates as Markers of Blood Pressure Using Invasive Pulse Transit Time Measurements as a Reference

4.1 Introduction

Pulse transit time (PTT) is the time it takes for the pressure or flow wave to propagate between two arterial sites. PTT measured as the time delay between invasive proximal and distal blood pressure or flow (BP or BF) waveforms (henceforth referred to as invasive PTT (I-PTT)) has been shown to correlate well with acute changes in BP over a wide physiological BP range [21][61][65][66]. PTT estimated as the time delay between non-invasive proximal and distal arterial waveforms could therefore permit convenient tracking of BP changes. Indeed, non-invasive PTT estimates are being widely pursued at present for cuff-less BP monitoring [55].

The most popular non-invasive PTT estimate has been the time delay between ECG and photoplethsymography (PPG) waveforms (henceforth referred to as pulse arrival time (PAT)) [55]. PAT has shown reasonably good correlation with systolic BP [55]. However, the major concern is that PAT not only includes PTT but also the pre-ejection period (PEP), which varies with cardiac electrical and mechanical properties. Another obvious, but hardly investigated, estimate is the time delay between proximal and distal PPG waveforms (henceforth referred to as PPG-PTT) [67] [68]. While this estimate eliminates the PEP concern, the timing of the PPG waveform, which indicates pulsatile blood volume, may not coincide with BP and BF waveforms due to viscoelastic delays, wave reflection, and/or other factors.

Despite the intense interest, the capabilities and limitations of these and other non-invasive PTT estimates in tracking BP changes are not yet fully understood. As outlined in [55], few studies have assessed non-invasive PTT estimates as markers of BP over a wide physiological BP range. Furthermore, few studies have compared different non-invasive PTT estimates in terms of their

ability to correlate with BP. Lastly, few studies have assessed non-invasive PTT estimates as markers of BP while using I-PTT as a reference, which may establish the upper bound on performance.

In this study, an animal model was used to compare PAT, PPG-PTT, and I-PTT in terms of tracking acute BP changes over a wide physiological BP range. The results showed that PPG-PTT was not significantly different from I-PTT and superior to the popular PAT as a marker of BP.

4.2 Materials and Methods

4.2.1 Data Collection

Experiments were performed in six healthy swine (30–40 kg). Each animal was studied on two separate days using procedures approved by the Michigan State University All-University Committee on Animal Use and Care.

Chronic instrumentation was installed during a sterile procedure as follows. Anesthesia was induced with an intravenous injection of propofol (2.2– 6.6 mg/kg) and maintained with inhaled isoflorane (1.5–2.5%), and mechanical ventilation was instituted. A left lateral thoracotomy was performed. An ultrasonic flow probe was placed around the ascending aorta for measurement of a proximal BF waveform (A-series, Transonic Systems, NY). The chest was evacuated and closed in layers, with the cable tunneled subcutaneously and exteriorized between the scapulae. The animal was then allowed several days for recovery.

Following the recovery period, anesthesia was likewise induced and maintained, and mechanical ventilation was instituted and adjusted to keep end-tidal CO_2 at 40-45 mmHg. Skin electrodes were positioned for measurement of the ECG waveform (ECG100C, Biopac, CA); a

micromanometer-tipped catheter was inserted into a femoral artery for measurement of a distal BP waveform (SPC-320, Millar Instruments, TX); an infrared, transmission-mode PPG clip was attached to the tongue (in the first four subjects) or an infrared, reflectance-mode PPG clip was attached to the skin on the neck (in the last two subjects) for measurement of a proximal PPG waveform (PPG100C, Biopac); and another infrared, reflectance-mode PPG clip was attached to the skin a few centimeters distal to the opposite femoral artery for measurement of a distal PPG waveform. Additional instruments were also placed to address aims unrelated to this study. The analog transducer outputs were interfaced to a personal computer via an analog-to-digital conversion system (MP150, Biopac). The measurements were then recorded at a sampling rate of 500 Hz over the course of 150 to 250 min during baseline conditions and intravenous infusions of dobutamine, diltiazem, phenylephrine, nitroprusside, and norepinephrine. Various infusion rates were employed followed by recovery periods.

4.2.2 Data Analysis

As shown in Figure 4-1, I-PTT was determined as the time delay between the proximal BF and distal BP waveforms; PPG-PTT was determined as the time delay between the proximal and distal PPG waveforms; and PAT was determined as the time delay between the ECG and distal PPG waveforms. The minimum, maximum double derivative, intersection of tangent lines, maximum derivative, and peak of the BF, BP, and PPG waveforms and the R-wave of the ECG waveform were automatically detected for each beat to establish multiple versions of each time delay [43][61]. Each version of each time delay was then computed over 1-min intervals by averaging the middle tertile of the values (for robustness against any artifact and misdetections) and plotted against the corresponding 1-min averages of diastolic, mean, and systolic BP for each subject. Linear, quadratic, cubic, logarithmic (including an intercept), and reciprocal (including

an intercept) functions were fitted to the data points in all of the plots. The degree of fit was quantified using the R^2 value. The version of each time delay and the function that yielded the best monotonic fit were selected. Finally, the group average R^2 values of the three time delays were compared for each BP level via one-way repeated measures ANOVA and the Tukey test for multiple comparisons.

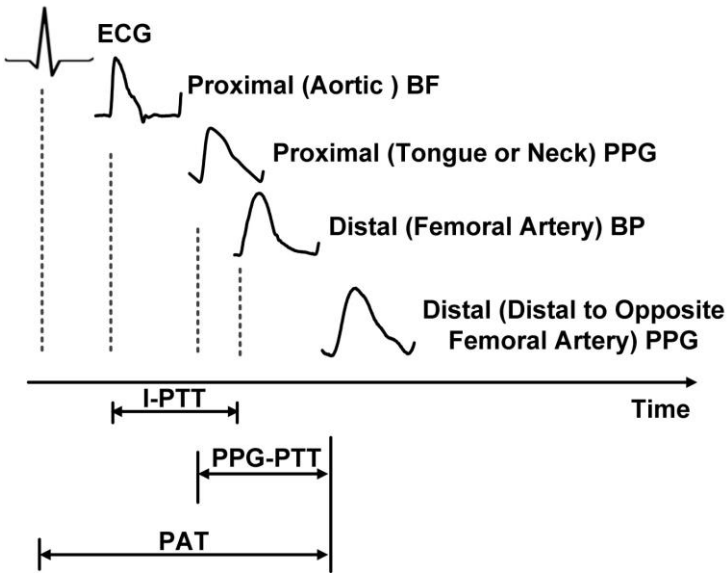

Figure 4-1 Determination of invasive pulse transit time (I-PTT), photoplethysmography-pulse transit time (PPG-PTT), and pulse arrival time (PAT) from arterial and ECG waveforms measured from six swine.
The proximal waveform for PPG-PTT was obtained using a tongue PPG clip for subjects 1 thru 4 and a neck PPG clip for subjects 5 and 6. BP and BF are blood pressure and blood flow, respectively.

4.3 Results

Figure 4-2 shows plots of mean BP versus each time delay per subject. The figure includes exponential functions of best fit, and the data points are color-coded to indicate the hemodynamic drug. The Table 6 shows the individual subject and group average (mean±SE) R^2 values between each time delay and each BP level. The R^2 values generally corresponded to

visual assessment of the degree of fitting and therefore served as a good quantitative index of BP tracking ability here.

The BP levels varied widely in each subject. That is, the group averages of the standard deviations of diastolic, mean, and systolic BP were 25±2, 29±2, and 36±2 mmHg, respectively.

The time delays were determined via waveform feet definitions. In particular, I-PTT was determined as the time delay between the maximal second derivatives of the proximal BF and distal BP waveforms; PPG-PTT was determined as the time delay between the minima of the proximal and distal PPG waveforms; and PAT was determined as the time delay between the R-wave of the ECG waveform and the maximal second derivative of the distal PPG waveform. Interchanging the maximal second derivative, minimum, or intersection of tangent lines of the waveforms with each other resulted in only modestly lower R^2 values for each time delay; however, use of the peak or maximum derivative of the waveforms yielded noticeably smaller R^2 values for all of the time delays (results not shown).

An exponential function generally provided the best monotonic fit of the data points in the plots of each BP level versus each time delay (results not shown). The exponential function was specifically of the form, $BP = A \cdot e^{B \cdot PTT}$.

As expected, I-PTT correlated tightly with BP. I-PTT, in fact, served as a strong marker of diastolic, mean, and systolic BP (group average R^2 values between 0.86±0.03 and 0.91±0.03) and was never a poor marker of any BP level in any subject (lowest R^2 value of 0.74).

PPG-PTT also correlated well with all three BP levels in each subject (group average R^2 values between 0.81±0.03 and 0.85±0.02). PPG-PTT was not significantly different from I-PTT as a

marker of each BP level (all p-values from comparisons of corresponding R^2 values were above 0.5). While PPG-PTT appeared to perform best and even better than I-PTT in the last two subjects with a neck rather than tongue PPG sensor, the improved performance could also be attributable to differences in the employed drugs and their effect in these particular subjects.

Consistent with previous findings, PAT correlated appreciably better with systolic BP (group average R^2 value of 0.70±0.04) than diastolic and mean BP (group average R^2 values of 0.49±0.07 and 0.60±0.06, respectively). However, PAT was inferior to both I-PTT and PPG-PTT as a marker of all three BP levels (all p-values from comparisons of corresponding R^2 values were less than 0.001 for I-PTT and 0.02 for PPG-PTT). PEP was clearly responsible for PAT's inferior correlation to BP. For example, both phenylephrine (green data points in Figure 4-2) and dobutamine (red data points in Figure 3-2) increased BP to similar levels. But, phenylephrine increased PEP by 10.4±7.3 msec relative to baseline conditions via enhanced afterload, whereas dobutamine decreased PEP by 30.1±6.0 msec relative to baseline conditions via enhanced contractility. As a result, PAT, which equals the sum of PTT and PEP, was particularly poor as a marker of high BP and could not always adequately track even systolic BP (lowest R^2 value of 0.51).

4.3.1 Discussion

In this study, PAT, PPG-PTT, and I-PTT were compared as markers of BP during infusions of various hemodynamic drugs in animals. By leveraging an animal model, this study may be the first to compare the ability of non-invasive PTT estimates in tracking BP changes over a wide physiological BP range using I-PTT measurements as a reference.

Table 6 Individual subject and group average correlation values beetween blood pressure (BP) levels and time delays

		Subject					
R^2		1	2	3	4	5	6
Diastolic BP	I-PTT	0.98	0.79	0.88	0.89	0.77	0.87
	PPG-PTT	0.79	0.79	0.67	0.78	0.89	0.94
	PAT	0.31	0.57	0.23	0.48	0.77	0.59
Mean BP	I-PTT	0.99	0.87	0.95	0.96	0.77	0.89
	PPG-PTT	0.84	0.79	0.77	0.79	0.89	0.96
	PAT	0.47	0.68	0.36	0.63	0.81	0.68
Systolic BP	I-PTT	0.93	0.95	0.94	0.94	0.74	0.88
	PPG-PTT	0.87	0.82	0.87	0.80	0.83	0.92
	PAT	0.63	0.81	0.51	0.70	0.82	0.73

		Diastolic BP	Mean BP	Systolic BP
p-value	I-PTT vs PPG-PTT	0.76	0.57	0.65
	I-PTT vs PAT	<0.001	<0.001	<0.01
	PPG-PTT vs PAT	<0.005	<0.01	<0.02

The R2 values indicate the degree of exponential fitting between each BP level and time delay. The p-values were obtained from the Tukey test for multiple comparisons, as one-way repeated measures ANOVA comparisons of the three time delays for each BP level always yielded $p < 0.05$. I-PTT is invasive pulse transit time, PPG-PTT is photoplethysmography-pulse transit time, and PAT is pulse arrival time (see Fig. 1 for further details).

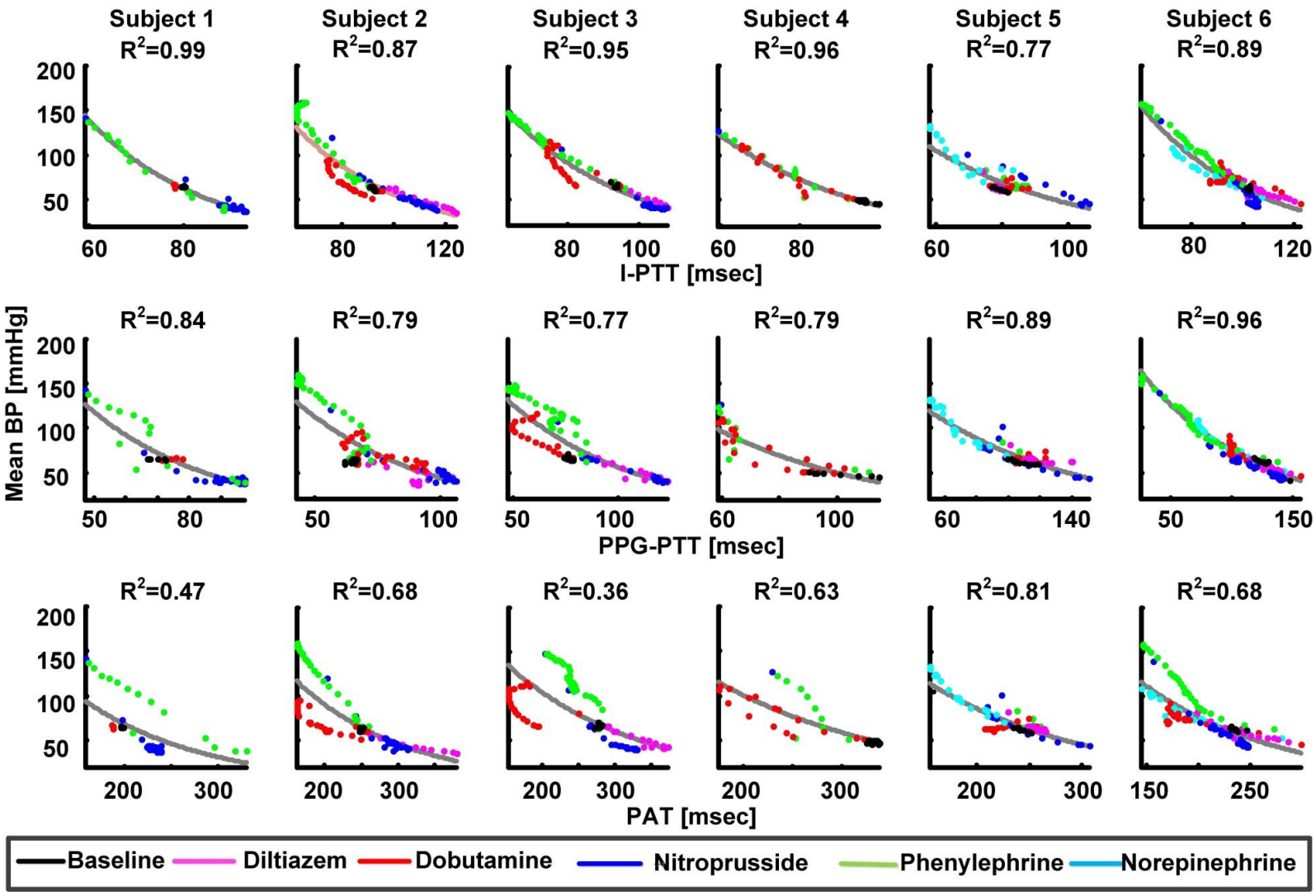

Figure 4-2 Plots of mean BP versus I-PTT, PPG-PTT, and PAT per subject along with best-fit exponential functions and corresponding R2 values.

More specifically, I-PTT was determined as the foot-to-foot time delay between invasive proximal BF and distal (femoral artery) BP waveforms; PPG-PTT was determined as the foot-to-foot time delay between proximal and distal (slightly distal to the opposite femoral artery) PPG waveforms; and PAT was determined as the time delay between the R-wave of the ECG waveform and the foot of the same distal PPG waveform (see Figure 4-1). Use of the peak or maximal derivative of the waveforms instead of the feet for establishing the time delays compromised their ability track all BP levels including systolic BP, which occurs near the waveform peaks (results not shown).

An exponential function better fit the data points in the plots of the BP levels versus the time delays than previously proposed functions such as $BP = A \cdot \ln(PTT)+B$ or $BP = (A/PTT)+ B$ [55](see Figure 4-2). This finding could be due to confounding factors that also influence PTT. For example, according to the Bramwell-Hill equation, PTT not only varies positively with arterial compliance but also inversely with the arterial cross-sectional area. The arterial cross-sectional area changes more per a unit change in BP in the low BP regime wherein parallel collagen fibers do not exert tension [55]. Hence, as BP decreases in the low BP regime, the arterial cross-sectional area may have been appreciably decreasing so as to cause PTT to increase more per unit change in BP in this regime as compared to the high BP regime.

Consistent with previous studies [21] [61][65][66], I-PTT correlated tightly with BP (see Figure 4-2). The group average R^2 values resulting from the exponential fitting between I-PTT and diastolic, mean, and systolic BP were between 0.86 ± 0.03 and 0.91 ± 0.03 (see Table 6). In theory, I-PTT should correlate best with diastolic BP, as it was determined from the waveform feet, which denotes diastolic BP. Since I-PTT showed similar correlations with mean and systolic BP, all three BP levels were clearly correlated with each other in this study.

Also consistent with previous studies [55], PAT correlated better with systolic BP than diastolic and mean BP (see Table 6). The reason for the result could be that PAT, which includes PEP in addition to PTT, and systolic BP are both determined by the ventricles and arteries. However, PAT was significantly inferior to I-PTT as a marker of the BP levels including systolic BP (group average R^2 values of 0.70±0.04 versus 0.90±0.03; $p < 0.01$). The reason for this result was, not surprisingly, the inclusion of PEP in PAT (see Figure 4-2). Interestingly, invasive PAT (the time delay between the R-wave of the ECG waveform and the foot of the distal BP waveform) was not as good a marker of the BP levels (group average R^2 values ranging from 0.22±0.09 to 0.37±0.08) as non-invasive PAT (results not shown). This result suggests that the time delay between the distal BP and PPG waveforms was nontrivial and correlated with BP (see below).

Similar to I-PTT, PPG-PTT correlated equally well with all BP levels. The group average R^2 values ranged from 0.81±0.03 and 0.85±0.02 (see Table 6 and Figure 4-2). These values were significantly higher than those for PAT even for systolic BP (group average R^2 values of 0.85±0.02 versus 0.70±0.04; $p < 0.02$) and not significantly different from those for I-PTT.

However, PPG-PTT and I-PTT were not identical. Figure 4-3 shows a break-down of plots of mean BP versus PPG-PTT into plots of mean BP versus the constituent time delays of PPG-PTT per subject. As indicated in Figure 4-1 and 4-3, PPG-PTT equals I-PTT minus the time delay between proximal BF and PPG waveforms plus the time delay between distal BP and PPG waveforms. The plots of mean BP versus the latter two time delays appeared similar, so these time delays may have partially canceled each other out in the formation of PPG-PTT. However, perhaps counter-intuitively, neither was relatively small nor independent of BP. These nontrivial

time delays may be caused by viscous effects. In particular, the path for wave travel here (e.g., from the femoral artery to skin vessels slightly distal to the femoral artery) consisted of very small arteries, which are governed by viscous BF. According to Womersley theory, the transit time in such arteries can increase with decreasing vessel radius [5]. (It should be noted, however, that this theory has been recently challenged [69] Alternatively or in addition, the peripheral arterial wall exhibits a significant viscous response in addition to an elastic response when loaded [55][70]. Such viscoelastic wall properties cause BP and blood volume to be dynamically related such that PPG, which is a metric of blood volume, can be delayed in time with respect to BP [26][55][70]. It is also worth mentioning that wave reflection could possibly have contributed to the genesis of the two nontrivial time delays. Finally, the dependency of these time delays on BP could potentially be attributable, at least in part, to the high degree of nonlinearity of the peripheral arterial compliance (see Figure 4-3 in [71]).

PPG-PTT was able to track diastolic, mean, and systolic BP in this study, because all three BP levels were well correlated here. While this correlation may be typical, there are conditions wherein diastolic and systolic BP do not change in parallel such as central hypovolemia induced by lower body negative pressure [72]. In such conditions, PPG-PTT may only be able to track diastolic BP, as it is determined from the waveform feet. However, based on the results of this study, PAT could possibly be a better marker of systolic BP in these conditions but not as good as PPG-PTT would be as a marker of diastolic BP.

PPG-PTT as well as PAT and I-PTT indicated wave travel time through central arteries here. In most previous studies, wave travel time through peripheral arteries, especially the time delay between ECG and finger PPG waveforms (i.e., finger PAT), was determined [55]. Since central arteries have less smooth muscle than peripheral arteries, wave travel time through central

arteries may be mainly dependent on BP, whereas wave travel time through peripheral arteries may depend on BP and confounding smooth muscle contraction [55]. For this reason, wave travel time through central arteries may be preferred.

In conclusion, the results of this study suggest that PPG-PTT should be explored in humans to achieve cuff-less BP monitoring. Use of ear and toe PPG sensors may be a sensible choice for determining PPG-PTT. One reason is that PPG waveforms can often be well measured from the ear and toe [73]. Another reason is that wave travel time through central arteries would be determined. Indeed, one previous study showed that PPG-PTT determined via ear and toe PPG sensors was able to track diastolic BP in surgical patient [67]. Further human studies are needed to confirm and extend these results. If PPG-PTT via ear and toe sensors proves sufficient in correlating with BP changes in humans, challenges will remain in calibrating the time delay in units of msec to BP in units of mmHg and creating a practical device. Note that such a device could not be used for chronic BP monitoring without periodic recalibration, as PTT through central arteries changes with aging and disease in addition to BP. Also note that even if calibration efforts were unsuccessful, PPG-PTT, by itself, may still permit tracking of relative changes in BP over time periods shorter than aging and disease processes (e.g., within a year) and may thus be useful for guiding anti-hypertensive therapy in individual patients.

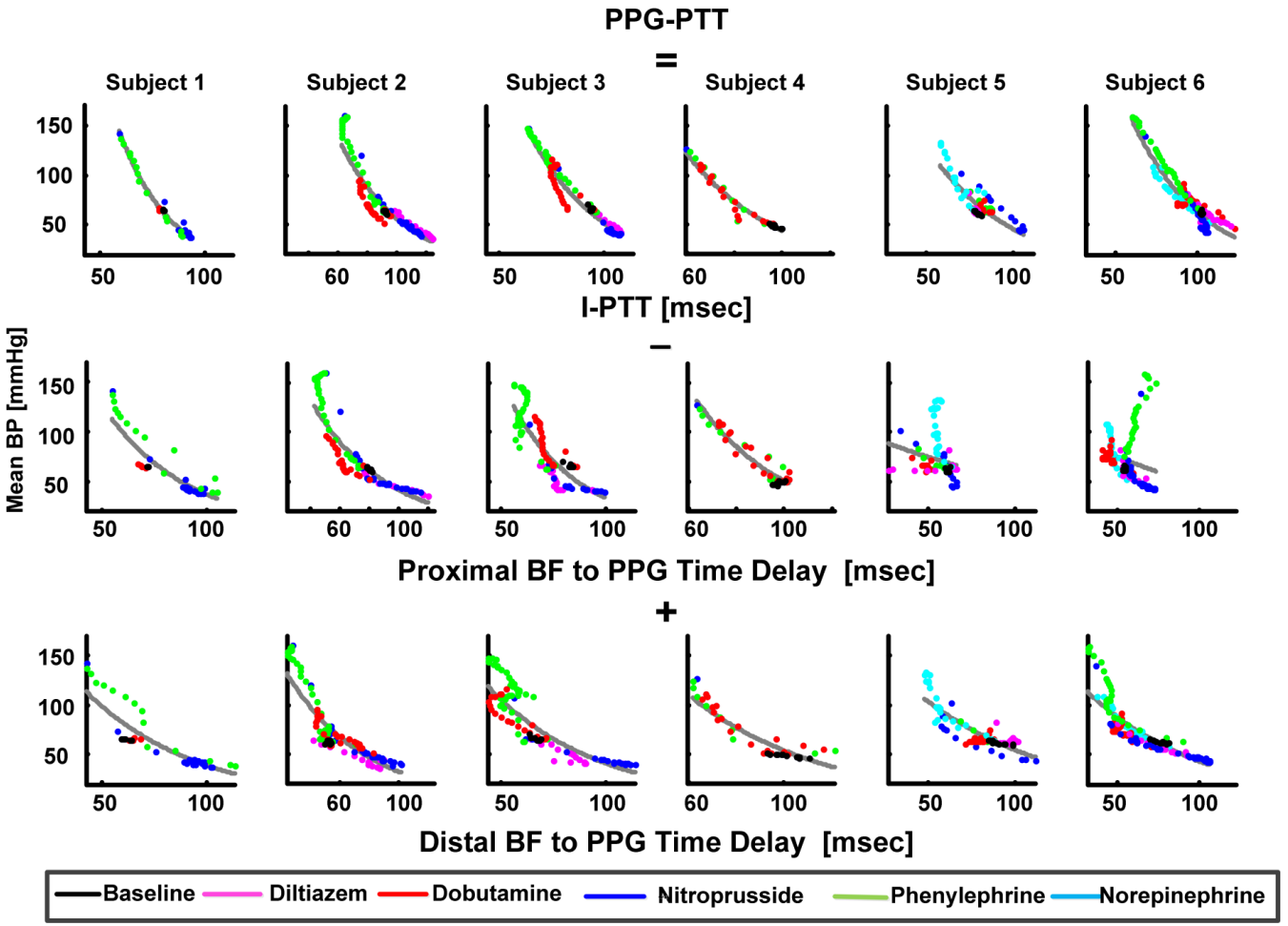

Figure 4-3 Break-down of plots of mean BP versus PPG-PTT into plots of mean BP versus the constituent time delays of PPG-PTT per subject.
The time delays between proximal BF and PPG waveforms and between distal BP and PPG waveforms were significant and dependent on BP. However, the plots of mean BP versus these time delays were similar, so the time delays partially canceled each other out in the formation of PPG-PTT.

Chapter 5. A Simple Adaptive Transfer Function for Deriving the Central Blood Pressure Waveform from a Radial Blood Pressure Waveform

5.1 Introduction

Central blood pressure (BP) is physiologically more relevant than radial BP and could therefore provide greater clinical value. However, the radial BP waveform is easier to measure via catheterization and applanation tonometry.

O'Rourke and co-workers previously proposed to mathematically derive the central BP waveform from a radial BP waveform using a generalized transfer function (GTF) [74]. Thereafter, some of us showed that the GTF could yield good agreement with invasive central BP measurements in cardiac catheterization patients [75][76]. These initial, independent validation studies have received considerable attention and helped popularize the GTF.

However, the GTF is a population average transfer function and therefore may not adapt well to the inter-subject and temporal variability in pulse pressure (PP) amplification (the ratio of radial PP to central PP) caused by, for example, BP- and age-induced changes in the wave travel time and peripheral resistance-induced changes in the wave reflection coefficient. As a result, it could be prone to nontrivial error. An improved transfer function could help enhance the clinical utility of central BP, which has only been able to demonstrate marginal added clinical value over peripheral BP up to now [11].

In this study, we conceived a new transfer function for deriving the central BP waveform from a radial BP waveform that can adapt to the arterial parameters of the subject at the time of measurement. First, the transfer function relating radial BP to central BP is defined in terms of an arterial model with two unknown parameters representing the wave travel time and wave

reflection coefficient. Then, the parameter values of the simple model are estimated by exploiting the frequent observation that central BP waveforms exhibit exponential diastolic decays [14][77][78][79]. The parameter values are continually updated for each subject so as to yield an "adaptive transfer function" (ATF). We compared the simple ATF to multiple GTFs using the original patient data that helped popularize the GTF. Our results showed that this ATF can offer significant accuracy improvements in the estimation of central BP levels in patients with low PP amplification.

5.2 Methods

5.2.1 Adaptive Transfer Function (ATF)

The ATF transforms a radial BP waveform into the central BP waveform based on physiologic modeling and knowledge. The procedure is shown in Figure 5-1 and described below.

A tube-load model is employed to represent arterial wave transmission and reflection (see Figure 5-1a). The tube represents the wave travel path between the ascending aorta and a radial artery, while the terminal load represents the arterial bed distal to the radial artery. (Note that the wave travel path to other peripheral arteries could be represented by placing similar combinations of tubes and loads in parallel.) The tube accounts for arterial inertance [L] and compliance [C] and therefore exhibits constant characteristic impedance [$Z_c = \sqrt{(L/C)}$] and allows waves to travel along the entire tube with constant time delay or wave travel time [$T_d = \sqrt{(LC)}$]. The load accounts for the peripheral resistance [R]. While previous tube-load models have represented the load with a more complicated, three-parameter Windkessel [49], the purely resistive load turned out to suffice here (see below). Waves traveling in the forward direction (left-to-right) along the tube

are reflected in the backward direction (right-to-left) at the terminal load with a constant reflection coefficient ($\Gamma = (R-Z_c)/(R+Z_c)$) so as to mimic the progressive amplification that BP waveforms undergo with increasing distance from the heart. According to this model, the transfer function relating a radial BP waveform [$p_r(t)$] (i.e., BP at the tube end) to the central BP waveform [$p_c(t)$] (i.e., BP at the tube entrance) may be defined in terms of two parameters, T_d and Γ (see transfer function equation in the time-domain in Figure 5-1a).

The two model parameters values, and thus the central BP waveform, are estimated from only the radial BP waveform sampled at 200 Hz by assuming that the central BP waveform exhibits exponential diastolic decays (see Figure 5-1b). First, values for T_d in the wide range of 0 to 150 ms, with increments of 5 ms, and Γ in the physical range of 0 to 1, with increments of 0.05, are selected. Second, a candidate central BP waveform is computed by applying the time-domain model equation, equipped with the two selected parameter values, to the radial BP waveform. Third, a 100-sample finite impulse response low-pass filter is applied to further smooth the candidate waveform. Fourth, the diastolic interval (DI) of each beat of the candidate central BP waveform is approximated from the preceding pulse length (PL) according to the following formula: $DI = PL - 0.4(1-e^{-2 \cdot PL})$ [80]. Fifth, the candidate central BP waveform over each DI is log transformed, and a line is fitted to these data using standard linear regression. Lastly, the average square fitting error over all of the beats is computed. These six steps are repeated for every pair of values in the T_d and Γ ranges to arrive at a set of candidate central BP waveforms. The T_d and Γ values and candidate central BP waveform that yield the minimum fitting error are chosen as the final estimates.

Fig. 1a

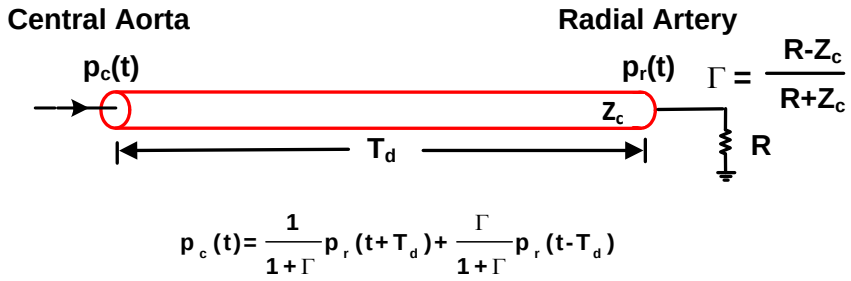

Fig. 1b

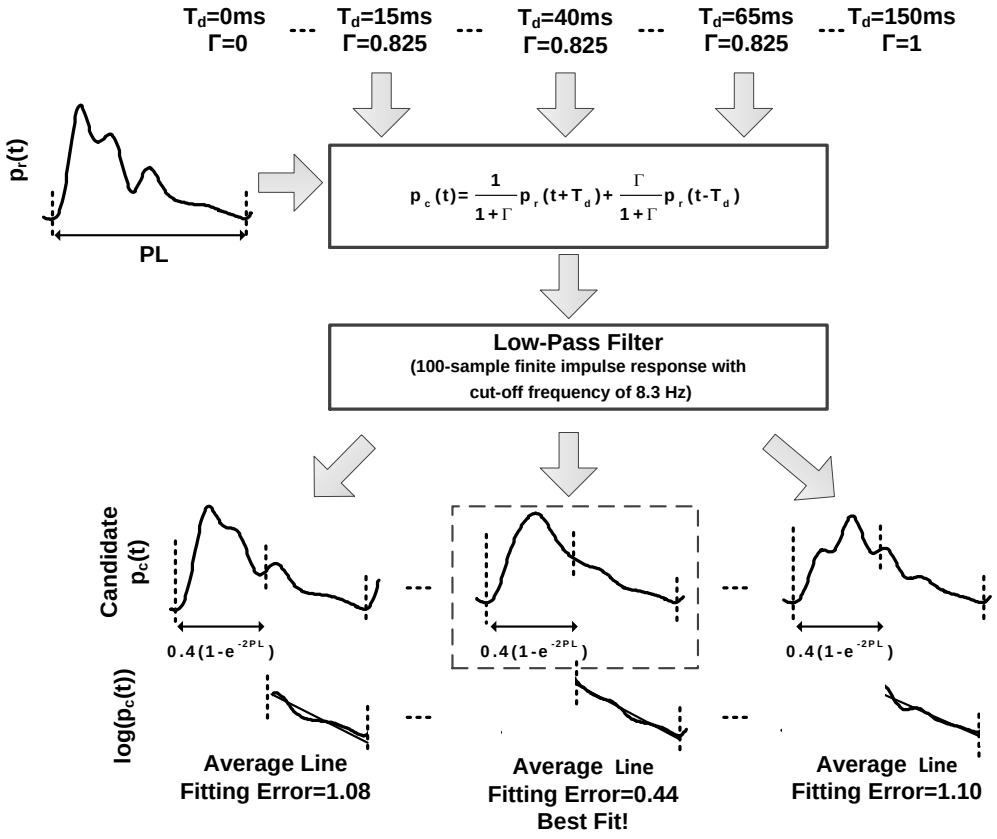

Figure 5-1 Adaptive transfer function (ATF) for deriving the central blood pressure (BP) waveform from a radial BP waveform.

(a) *The transfer function relating radial BP [$p_r(t)$] to central BP [$p_c(t)$] is defined in terms of the wave travel time [T_d] and wave reflection coefficient [Γ] parameters of an arterial tube-load model. Z_c is the arterial characteristic impedance, and R is peripheral resistance.* ***(b)*** *The model parameters, and thus the central BP waveform, are estimated by making the waveform exhibit maximally exponential diastolic decays. PL is pulse length.*

5.2.2 Patient Data

The ATF was assessed and compared to GTFs using patient data that some of us previously collected under institutional review board approval from the Johns Hopkins Hospital and originally used for initial, independent validation of the GTF. These data are described in detail elsewhere [75][76]. Briefly, the data were from two cohorts of cardiac catheterization patients. The first cohort comprised 20 patients with a hemodynamic intervention to transiently change BP in 14 of the subjects [75]. The second cohort consisted of 19 patients without any intervention [76]. Each patient record included a radial BP waveform via an applanation tonometer and the reference central BP waveform via a micromanometer-tipped ascending aortic catheter. Both waveforms were 10-35 sec in duration, sampled at 200 Hz, and low-pass filtered with a cutoff frequency of 15 Hz. Three of the interventions produced changes in central BP levels that lasted less than 10 beats. Since the ATF and perhaps even the GTF require steady periods of data for their construction, the post-intervention waveforms for the corresponding patient records were excluded from subsequent data analysis. Table 7 summarizes the patient and data characteristics.

5.2.3 Data Analysis

Similar to the original, independent validation studies of the GTF [75][76], the radial BP waveforms were calibrated to the mean and diastolic levels of the reference central BP waveforms in order to focus on the transfer function itself in absence of the confounding effect of the BP calibration (see Discussion section). The patient records in the first cohort were used to train the ATF and GTFs, while the patient records in the second cohort were used to test the transfer functions. The roles of the first and second cohorts

Table 7 Patient and data characteristics

Patient Characteristics	Cohort 1 (n=20)	Cohort 2 (n=
Men [%]	80	74
Age [years]	59±11	51±16
Post Heart Transplant [%]	50	26
Coronary Artery Disease [%]	10	58
Dilated Cardiomyopathy [%]	35	0
Constrictive Pericarditis [%]	5	0
Normal [%]	0	11
Hypertension [%]	0	5
Data Characteristics (Baseline)	**Cohort 1 (n=20)**	**Cohort 2 (n=**
Central SP [mmHg]	145±23	127±27
Central PP [mmHg]	59±15	48±17
Radial PP [mmHg]	69±28	52±11
DP [mmHg]	86±15	79±18
Data Characteristics (Intervention)	**Cohort 1 (n=11)**	**Cohort 2 (n=**
Valsalva Maneuver [%]	55	-
Nitroglycerin [%]	9	-
Abdominal Compression [%]	27	-
Inferior Vena Cava [%]	9	-
|Central SP Change| [mmHg]	31±20	-
|Central PP Change| [mmHg]	16±11	-
|Radial PP Change| [mmHg]	14±12	-
|DP Change| [mmHg]	24±15	-

Values are mean±SD or percentages. PP is pulse pressure; SP, systolic pressure, DP, diastolic pressure, |X Change|, absolute value of X change induced by intervention relative to baseline.

Table 8 Root-mean-squared-errors between estimated and measured central blood pressure (BP)

Central BP Estimates	Low PP Amplification (1.06±0.07)			Middle PP Amplification (1.25±0.07)			High PP Amplification (1.59±0.13)		
	TW	SP	PP	TW	SP	PP	TW	SP	PP
Radial BP	6.6*	6.1#	6.1	7.8*	13.9*	13.9*	8.1*	21.6*	21.6*
$GTF_{SphygmoCor}$	4.7*	7.5*	10.1*	3.5	5.4	7.9*	2.9	3.1	4.8
GTF_{ARX}	5.2*	6.2#	7.1*	3.2	3.5	4.6	2.9	3.5	4.3
ATF	3.5	3.3	4.2	3.5	3.3	3.4	3.1	3.7	3.7

PP amplification is the ratio of radial to central pulse pressure; $GTF_{SphygmoCor}$, generalized transfer function (GTF) that mimics the SphygmoCor device; GTF_{ARX}, effective, autoregressive exogenous input-based GTF; ATF, adaptive transfer function in Figure 1; TW, total waveform; SP, central systolic pressure; and PP, central pulse pressure. * and # denote statistically different (e.g., $p < 0.05$) or borderline statistically different (e.g., $p \approx 0.05$) compared to ATF, respectively.

were then interchanged, and the training and testing procedure was repeated. In this way, the patient records in both cohorts were utilized to assess the transfer functions without employing the same data for training and testing.

The ATF was trained in terms of the cutoff frequency of the post-low-pass filter and the type of load (resistor versus three-parameter Windkessel [49]. For comparison, three GTFs were also trained. The first GTF was constructed based on the autoregressive exogenous input (ARX) identification procedure outlined in the original, independent validation study [76]. This procedure was shown to be most effective amongst various approaches in that study. The second GTF was constructed based on a more straightforward ARX identification procedure. In particular, one half of each pair of radial and central BP waveforms was utilized to determine the time delay ranging from -30 to 0 samples and the ARX parameters for model orders ranging from 1 to 15 using standard least squares estimation [40]. The other half of each pair of waveforms was then employed to determine which of the 15 ARX-based transfer functions yielded the minimum average square central BP waveform estimation error [40]. The optimal

transfer functions from each pair of waveforms were then averaged to arrive at the final GTF. This second GTF (GTF_{ARX}) estimated central BP more accurately than the first GTF in the testing data, and varying its model order range did not further improve the estimation (results not shown). The third GTF was built by reverse engineering the SphygmoCor device (AtCor Medical, Australia) (see Appendix). This GTF ($GTF_{SphygmoCor}$) was a 34-sample finite impulse response filter at a sampling frequency of 128 Hz that was virtually identical to the device transfer function (results not shown). The $GTF_{SphygmoCor}$ was thus investigated after resampling the waveforms to 128 Hz.

The testing data was divided into low, middle, and high PP amplification groups of equal sizes, and the following analysis was applied to each group. The central BP waveforms estimated by the ATF, GTF_{ARX}, and $GTF_{SphygmoCor}$ were quantitatively evaluated against the reference central BP waveforms in terms of the sample-to-sample (total waveform, TW), average systolic BP (SP), average PP, average augmentation index, and average ejection interval root-mean-squared-errors (RMSEs). The analyzed radial BP waveforms were likewise evaluated. All waveforms were time aligned with the reference waveforms prior to the TW RMSE calculation. The RMSEs for the ATF were then statistically compared to the RMSEs for the two GTFs and the radial BP waveform via paired t-tests of the squared-errors with Holm's correction for the three comparisons [81]. In addition, the T_d and Γ estimates of the ATF were statistically compared between pairs of the three PP amplification groups via two-sample t-tests again with Holm's correction for the three comparisons.

5.3 Results

The ATF implemented with a purely resistive load performed essentially the same as the ATF implemented with a conventional three-parameter Windkessel load in the training data. Hence,

the simpler load was selected. The post-low-pass filter cutoff frequency for the ATF was 8.4 Hz when the first cohort of patient records was used as the training data and 7.9 Hz when the second cohort was used as the training data. Hence, despite the use of two training datasets, the ATF could be represented with a single procedure, as shown in Figure 5-1b. Note that a post-low-pass filter did not improve the central BP estimates of the GTFs.

Table 8 shows the central TW, SP, and PP RMSEs for the radial BP waveform, $GTF_{SphygmoCor,}$ GTF_{ARX}, and ATF in the testing data for the low, middle, and high PP amplification groups. The average (mean±SD) PP amplification was 1.06±0.07 for the low group, 1.25±0.07 for the middle group, and 1.59±0.13 for the high group. The augmentation index and ejection interval RMSEs were not included in the table, because these RMSEs did not statistically differ amongst the three transfer functions.

As expected, the RMSEs for the radial BP waveform were very large but decreased substantially with decreasing PP amplification. The RMSEs for the $GTF_{SphygmoCor}$ were lowest in the high PP amplification group rather than the middle PP amplification group and were highest in the low PP amplification group. Also as expected, the RMSEs for the GTF_{ARX} were low in the middle PP amplification group and higher in the low PP amplification group. However, this transfer function surprisingly yielded low RMSEs for the high PP amplification group. By contrast, the RMSEs for the ATF were comparable in all three PP amplification groups. Further, the RMSEs for the ATF were considerably lower than those for the radial BP waveform in all three groups, significantly lower than those for both GTFs in the low PP amplification group, and even lower than those for the $GTF_{SphygmoCor}$ in the middle PP amplification group. Most notably, in the low PP amplification group, the ATF showed average RMSE reductions of 40% relative to the GTF_{ARX} and nearly 50% relative to the $GTF_{SphygmoCor}$.

Figure 5-2 shows representative examples of the estimated and measured central BP waveforms in the testing data for the low, middle, and high PP amplification groups. As can be seen, the ATF provided the best central BP waveform estimates over all three examples.

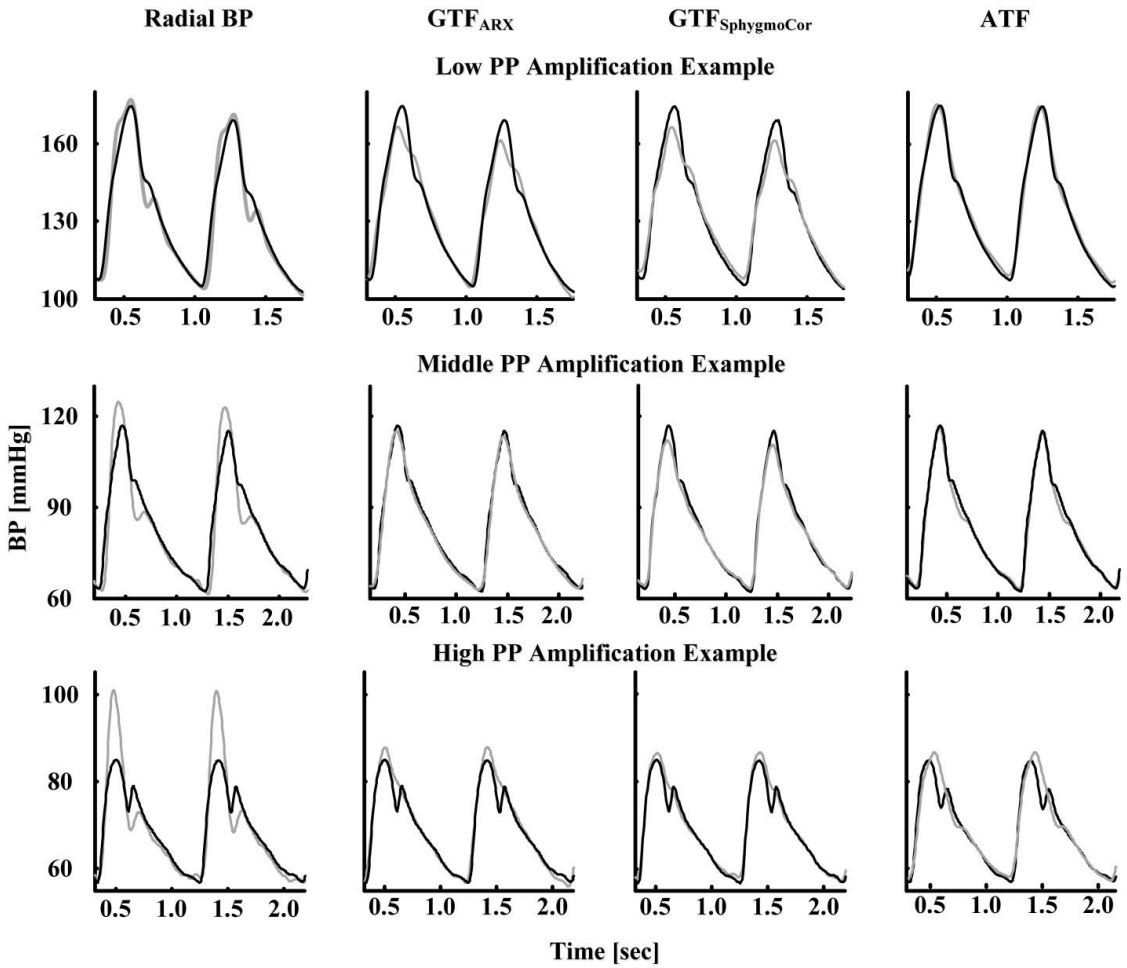

Figure 5-2 Representative examples of the estimated (gray) and measured (dark) central BP waveforms.
GTF_{ARX} is an effective, autoregressive exogenous input-based generalized transfer function (GTF), whereas $GTF_{SphygmoCor}$ is a GTF that mimics the SphygmoCor device. PP amplification is the ratio of radial to central pulse pressure.

Figure 5-3 shows the average T_d and Γ estimates of the ATF in the testing data for the low, middle, and high PP amplification groups. The T_d estimates significantly increased with PP

amplification, whereas the Γ estimates did not change. Since PP amplification can increase with T_d, Γ, or T_d and Γ, these parameter estimates give further credence to the ATF.

5.4 Discussion

We developed a simple adaptive transfer function (ATF) for mathematically deriving the central BP waveform from a radial BP waveform. The transfer function is defined in terms of the wave travel time and wave reflection coefficient parameters of a physical model of arterial wave transmission and reflection (see Figure 5-1a). The model parameters are then estimated from only the radial BP waveform by assuming that the central BP waveform exhibits exponential diastolic decays (see Figure 5-1b). In this way, unlike conventional GTFs, the transfer function may effectively adapt to the arterial properties of the subject at the time of measurement.

Over a century ago, Frank proposed that central BP waveforms could be represented with a Windkessel model, which predicts exponential diastolic decays [77]. Thereafter, exponential diastolic decays in the central BP waveform have been repeatedly observed [14][78][79]. The mechanism for such diastolic decays may be as follows [82]. Forward and backward waves in the aorta have large phasic differences due to the long and varying distances between the aorta and the main reflection sites at the arterial terminations. Hence, waves with short wavelengths tend to cancel each other out in the aorta. On the other hand, waves with longer wavelengths build up in the aorta. However, these wavelengths may be long relative to the dimension of the arterial tree such that it indeed acts like a Windkessel from the perspective of the aorta. The physical model upon which the ATF is based captures this mechanism to a significant, but incomplete, extent [82].

In a previous study, we proposed another ATF that employed the same physical model but instead estimated the model parameters by exploiting the fact that central (ascending aortic)

blood flow is negligible during diastole [36]. We also showed that this ATF could yield more accurate central BP estimates than GTFs when applied to femoral BP waveforms from animals. However, the systolic upstroke-downstroke intervals of the patient radial BP waveforms studied herein were often narrower than those of the femoral BP waveforms. As a result, our original ATF sometimes predicted central blood flow waveforms with diastolic intervals that were too wide in this study. Our conclusion is that the simple physical model (see Figure 5-1a) may be more valid for the radial BP-to-central BP transfer function than the radial BP-to-central blood flow transfer function. We also mention that the new and simpler ATF described herein has similarity to another previously proposed ATF, which again used the same physical model but estimated the model parameters by assuming that the central BP waveform was maximally smooth throughout the cardiac cycle [34].

We assessed the ATF and compared it to GTFs using the same patient data that helped popularize the GTF [75][76]. These data included gold standard reference central BP waveforms in addition to non-invasive radial BP waveforms from 39 cardiac catheterization patients as well as some interventions to vary BP (see Table 7). Our specific hypothesis was that changes in PP amplification (the ratio of radial PP to central PP) would adversely impact the GTFs but not the ATF. So, we divided the patient data into low, middle, and high PP amplification groups of equal sizes and studied the transfer function performance per group (see Table 8)

The $GTF_{SphygmoCor}$, which was able to mimic the SphygmoCor device, estimated central BP most accurately in the high, rather than middle, PP amplification group. The reason may be that the device was trained using central and radial BP waveforms from a large number of relatively healthy subjects but of similar average age as the patients studied herein [83]. Hence, the performance of the $GTF_{SphygmoCor}$ degraded with decreasing PP amplification and became

relatively poor in the low PP amplification group. These results suggest that the SphygmoCor device may possibly be biased toward normal subjects.

The GTF_{ARX}, which was trained using the same data and in the same way as the ATF, accurately estimated central BP in the middle PP amplification group, as expected. Its performance degraded in the low PP amplification group but was surprisingly good in the high PP amplification group. Hence, although GTFs are population averages, they have some ability to adapt to variations in PP amplification by virtue of being frequency selective.

The ATF accurately estimated central BP in all three PP amplification groups. Further, its performance was significantly better than both GTFs (see Figure 5-2). Most notably, in the low PP amplification group, the ATF was able to reduce the central TW, SP, and PP estimation errors by an average of nearly 50% compared to the $GTF_{SphygmoCor}$ and 40% compared to the GTF_{ARX}. The low PP amplification group may not be an insignificant one. This group, by definition, constituted one-third of the patient data herein. Further, low PP amplification may occur with hypertension and aging [84] and is caused by a short wave travel time to the radial artery and/or a small wave reflection coefficient.

The wave travel time (T_d) estimates of the ATF indeed decreased with decreasing PP amplification, while the wave reflection coefficient (Γ) estimates did not change (see Figure 5-3). However, we note that the T_d estimates may be more reliable, because the transfer function is often relatively insensitive to Γ. In particular, the magnitude response of the transfer function is given as follows:

$$\sqrt{\cos^2(2\pi T_d f) + \left(\frac{1-\Gamma}{1+\Gamma}\right)^2 \sin^2(2\pi T_d f)}$$

where f is frequency. Hence, the transfer function is specifically insensitive to Γ for small f (e.g., < 3 Hz, which is a crucial frequency band) and moderate to high Γ (e.g., > 0.4) and becomes even more insensitive to Γ with decreasing T_d. Assuming Γ is relatively unimportant, if T_d is small, then the central BP waveform derived by the ATF will appear like the radial BP waveform, which nominally does not exhibit exponential diastolic decays. On the other hand, if T_d is large, then the derived central BP waveform will show double peaks rather than a smooth decay. Invoking the central BP exponential diastolic decay assumption may balance these two parameter settings so as to yield the proper T_d value. That is, if T_d were actually small (i.e., large pulse wave velocity), then the radial and central BP waveforms may both exhibit similar exponential diastolic decays, and the ATF would thus correctly yield a small T_d value. But, if T_d were actually large, then the radial BP waveform may not show an exponential diastolic decay, and the ATF would thus correctly yield a larger T_d value. In this way, the ATF was accurate over a wide range of PP amplifications.

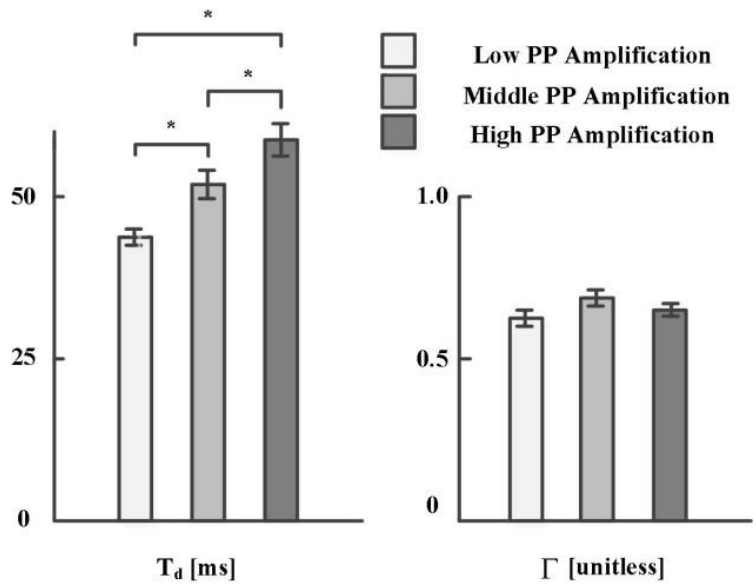

Figure 5-3 T_d and Γ (mean±SE) estimates of the ATF.
** Indicates statistical significance via two-sample t-tests with Holm's correction for multiple comparisons*

However, the ATF was not able to offer any improvement in the estimation of the augmentation index and ejection interval of the central BP waveform (results not shown). The reason may be that its underlying physical model is characterized by only two parameters and is therefore too simple to account for the detailed features of the central BP waveform.

An important issue left unaddressed is practical calibration of radial BP waveforms via applanation tonometry. Like the original GTF validation studies [75][76], we calibrated the radial BP waveforms with the reference central BP waveforms in order to focus on the transfer function. However, a major source of error in non-invasive central BP estimates is calibration with error-prone brachial BP measurements via current oscillometric cuff devices [85][86]. More accurate automatic cuff BP measurement methods are therefore also needed. Some of us have proposed such a method recently [56] and hope to combine it with the simple ATF introduced herein to achieve accurate, non-invasive central BP monitoring in practice.

5.5 Perspectives

PP and SP become amplified with increasing distance from the heart. The extent of the amplification varies with the wave travel time and wave reflection coefficient. So, it is central BP that truly reflects cardiac performance. Further, central BP rather than peripheral BP is a major determinant of the degenerative changes that occur in aging and hypertension [87]. Because of its greater physiologic relevance, central BP could provide superior clinical value. Several studies have compared central BP and peripheral BP in terms of predicting target organ damage and cardiovascular outcomes [11][29][88]. Overall, these studies have shown that central BP does offer greater clinical value, but the improvement is not as much as one may expect. One possible reason is nontrivial central BP measurement error. That is, in almost all of the studies, central BP was obtained by applanating a carotid artery with a tonometer, which is

difficult due to surrounding loose tissue, or applying a GTF, which ignores variations in the wave travel time and wave reflection coefficient, to a more easily measured radial BP waveform. The idea of the simple ATF introduced herein is to account for such variations by employing physiologic modeling and knowledge and thereby improve central BP measurement accuracy. Indeed, this ATF estimated central BP levels with significantly greater accuracy than GTFs in patients with low PP amplification while showing similar accuracy in patients with higher PP amplification. Future studies by independent investigators may be worthwhile to confirm these results and determine if the ATF can offer added clinical value.

APPENDIX

APPENDIX

The SphygmoCor device derives the central BP waveform by applying a GTF to a radial BP waveform via an applanation tonometer. To determine the GTF used by the device, fifteen recordings from five subjects were analyzed. For each recording, the device generated an average radial BP waveform and an estimated central BP waveform, both sampled at 128 Hz. The two waveforms were given in arbitrary units, although they may be calibrated with systolic and diastolic BP measurements from an arm cuff.

The central BP waveform [$p_c(t)$] was assumed to be estimated from the radial BP waveform [$p_r(t)$] via a finite impulse response filter as follows:

$$p_c(t) = \sum_{k=1}^{M} h(k) p_r(t-k),$$

where the filter samples are denoted by h(k), k = 1, …, M, and M is the number of samples or model order. MATLAB's system identification toolbox, and the arx function in particular, was used to determine the values of the filter samples. The model order was not known, so a variety of orders was investigated. The energy of the residual error of the central BP waveform estimated from the radial BP waveform was then observed as a function of the model order. As expected, the residual error energy decreased monotonically as the model order increased. When the model order reached 34, the residual error energy dropped abruptly to essentially zero and did not change with further increases in the model order. In addition, the magnitude of the first sample of the impulse response was smaller, by a factor of three, than the next smallest sample. Therefore, models with a delay of one sample (i.e., h(1) = 0) were investigated. The residual error energy dropped sharply to a value essentially equal to zero when there were 33 or more non-zero samples in the filter. The addition of more delay terms increased the residual error

energy. Further, the addition of up to six denominator terms, which yields an infinite impulse response, did not significantly reduce the residual error compared to a finite impulse response. In sum, the GTF used by the Sphygmocor device is evidently a finite impulse response filter with a delay of one sample and 33 non-zero samples whose values were accurately determined from the pair of BP waveforms outputted by the device.

Chapter 6. Future Work

Work remains to be done to improvement the monitoring of arterial stiffness and blood pressure in the following aspects accuracy, convenience and clinical relevance.

To be specific, different sensors and different signal processing techniques are to be explored to achieve the measurements of arterial stiffness or pulse wave velocity with better accuracy, improved accessibility and more clinical relevance, so that arterial stiffness can contribute more as guidance to stratify patients for better treatments.

Meanwhile for cuffless and continuous blood pressure monitoring, the calibration curve between blood pressure and pulse wave velocity measured non-invasively remains to be done in an easy and perturbationless manner. This can be a game changer in the patient monitoring domain.

Last but not the least, one direction to popularize the clinical measurement of central blood pressure is to measure commonly available blood pressure waveform from cuff to further estimate central blood pressure waveforms. To be able to achieve this can enable conventional cuff based blood pressure monitor provide central blood pressure information in addition to currently available brachial blood pressure information. The extra information can potentially improve the patient diagnosis and treatment for better clinical outcome.

BIBLIOGRAPHY

BIBLIOGRAPHY

[1] D. L. Hoyert and J. Xu, "Deaths : Preliminary Data for 2011," *Natl. Vital Stat. Reports*, vol. 61, no. 6, 2012.

[2] K. C. Fleming, J. M. Evans, and D. S. Chutka, "Caregiver and clinician shortages in an aging nation.," *Mayo Clin. Proc.*, vol. 78, no. 8, pp. 1026–40, Aug. 2003.

[3] R. Mukkamala and D. Xu, "Continuous and less invasive central hemodynamic monitoring by blood pressure waveform analysis," *Am. J. Physiol. Circ. Physiol.*, vol. 299, no. 3, pp. H584–H599, 2010.

[4] A. C. Guyton and J. E. Hall, *Textbook of Medical Physiology*. Philadelphia: W.B. Saunders Company, 1996.

[5] W. Milnor, *Hemodynamics*. Baltimore: Williams & Wilkins, 1982.

[6] J. C. Bramwell and A. V. Hill, "The velocity of the pulse wave in man," *Proc. R. Soc. London Ser. B-Containing Pap. a Biol. Character*, vol. 93, no. 652, pp. 298–306, 1922.

[7] A. U. Ferrari, A. Radaelli, and M. Centola, "Invited review: Aging and the cardiovascular system," *J. Appl. Physiol.*, vol. 95, no. 6, pp. 2591–2597, Dec. 2003.

[8] K. Hirata, M. Kawakami, and M. F. O'Rourke, "Pulse wave analysis and pulse wave velocity - A review of blood pressure interpretation 100 years after Korotkov," *Circ. J.*, vol. 70, no. 10, pp. 1231–1239, Oct. 2006.

[9] H. Y. Lee and B. H. Oh, "Aging and Arterial Stiffness," *Circ. J.*, vol. 74, no. 11, pp. 2257–2262, 2010.

[10] G. Mancia, R. Fagard, K. Narkiewicz, and J. Redon, "2013 ESH/ESC guidelines for the management of arterial hypertension: the Task Force for the Management of Arterial Hypertension of the European Society of Hypertension (ESH) and of the European Society of Cardiology (ESC).," *Eur. Heart J.*, vol. 34, no. 28, pp. 2159–219, Jul. 2013.

[11] C. Vlachopoulos, K. Aznaouridis, and C. Stefanadis, "Prediction of cardiovascular events and all-cause mortality with arterial stiffness: a systematic review and meta-analysis.," *J. Am. Coll. Cardiol.*, vol. 55, no. 13, pp. 1318–27, Mar. 2010.

[12] P. Boutouyrie, S. Laurent, and M. Briet, "Importance of arterial stiffness as cardiovascular risk factor for future development of new type of drugs," *Fundam. Clin. Pharmacol.*, vol. 22, no. 3, pp. 241–246, 2008.

[13] W. W. Nichols and M. F. O'Rourke, *McDonal's Blood Flow in Arteries*, 5th ed. Hodder Arnold, a member of the Hodder Headline Group, 2005.

[14] A. Noordergraaf, *Circulatory System Dynamics*. New York: Academic Press, 1978.

[15] S. Söderström, G. Nyberg, M. F. O'Rourke, J. Sellgren, J. Pontén, S. Soderstrom, and J. Ponten, "Can a clinically useful aortic pressure wave be derived from a radial pressure wave?," *Br. J. Anaesth.*, vol. 88, no. 4, pp. 481–488, Apr. 2002.

[16] J. Sola, S. F. Rimoldii, and Y. Allemann, "Ambulatory monitoring of the cardiovascular system: the role of Pulse Wave Velocity," in *New Developments in Biomedical Engineering*, 2010, pp. 391–424.

[17] P. Boutouyrie, S. Laurent, and M. Briet, "Determinants of pulse wave velocity in healthy people and in the presence of cardiovascular risk factors: 'establishing normal and reference values'.," *Eur. Heart J.*, vol. 31, no. 19, pp. 2338–50, Oct. 2010.

[18] J. Sugawara, K. Hayashi, Y. Yokoi, and H. Yanaka, "Carotid-Femoral Pulse Wave Velocity: Impact of Different Arterial Path Length Measurements," *Artery Res.*, vol. 4, no. 1, pp. 27–31, 2010.

[19] J. Blacher, a. P. Guerin, B. Pannier, S. J. Marchais, M. E. Safar, and G. M. London, "Impact of Aortic Stiffness on Survival in End-Stage Renal Disease," *Circulation*, vol. 99, no. 18, pp. 2434–2439, May 1999.

[20] A. P. Guerin, J. Blacher, B. Pannier, S. J. Marchais, M. E. Safar, and G. M. London, "Impact of Aortic Stiffness Attenuation on Survival of Patients in End-Stage Renal Failure," *Circulation*, vol. 103, no. 7, pp. 987–992, Feb. 2001.

[21] J. D. Pruett, J. D. Bourland, and L. A. Geddes, "Measurement of Pulse-Wave Velocity Using a Beat-Sampling Technique," *Ann. Biomed. Eng.*, vol. 16, no. 4, pp. 341–347, 1988.

[22] M. Proença, a Falhi, D. Ferrario, O. Grossenbacher, J. Porchet, J. Krauss, and J. Sola, "Continuous non-occlusive blood pressure monitoring at the sternum.," *Biomed. Tech. (Berl).*, vol. 57, pp. 2–5, Aug. 2012.

[23] H. Gesche, D. Grosskurth, G. Küchler, and A. Patzak, "Continuous blood pressure measurement by using the pulse transit time: comparison to a cuff-based method.," *Eur. J. Appl. Physiol.*, vol. 112, no. 1, pp. 309–15, Jan. 2012.

[24] Y. Choi, Q. Zhang, and S. Ko, "Noninvasive cuffless blood pressure estimation using pulse transit time and Hilbert–Huang transform," *Am J Hypertens*, vol. 24, no. (12), pp. 1312–1317, Jan. 2011.

[25] A. C. Burton, "Relation of Structure to Function of the Tissues of the Wall of Blood Vessels," *Physiol. Rev.*, vol. 34, no. 4, pp. 619–642, 1954.

[26] D. H. Bergel, "The Dynamic Elastic Properties of the Arterial Wall," *J. Physiol.*, pp. 458–469, 1961.

[27] P. Lantelme, C. Mestre, M. Lievre, A. Gressard, and H. Milon, “Heart Rate: An Important Confounder of Pulse Wave Velocity Assessment,” *Hypertension*, vol. 39, no. 6, pp. 1083–1087, Jun. 2002.

[28] C. S. Hayward, A. P. Avolio, and M. F. O’Rourke, “Arterial Pulse Wave Velocity and Heart Rate,” *Hypertension*, vol. 40, no. 6, p. 8e–9, Oct. 2002.

[29] T. K. Waddell, A. M. Dart, T. L. Medley, J. D. Cameron, and B. A. Kingwell, “Carotid pressure is a better predictor of coronary artery disease severity than brachial pressure,” *Hypertension*, vol. 38, no. 4, pp. 927–931, 2001.

[30] W.-C. Yu, S.-Y. Chuang, Y.-P. Lin, and C.-H. Chen, “Brachial-ankle vs carotid-femoral pulse wave velocity as a dterminant of cardiovascular structure and function,” *J. Hum. Hypertens.*, vol. 22, no. 1, pp. 24–31, Jan. 2008.

[31] J. Blacher, B. Pannier, a. P. Guerin, S. J. Marchais, M. E. Safar, and G. M. London, “Carotid Arterial Stiffness as a Predictor of Cardiovascular and All-Cause Mortality in End-Stage Renal Disease,” *Hypertension*, vol. 32, no. 3, pp. 570–574, Sep. 1998.

[32] G. Zhang, M. Gao, and R. Mukkamala, “Robust, beat-to-beat estimation of the true pulse transit time from central and peripheral blood pressure or flow waveforms using an arterial tube-load model,” *2011 Annu. Int. Conf. IEEE Eng. Med. Biol. Soc.*, vol. 2011, pp. 4291–4294, 2011.

[33] J.-O. Hahn, A. T. Reisner, and H. H. Asada, “Estimation of pulse transit time using two diametric blood pressure waveform measurements.,” *Med. Eng. Phys.*, vol. 32, no. 7, pp. 753–9, Sep. 2010.

[34] J.-O. Hahn, A. T. Reisner, F. a Jaffer, and H. H. Asada, “Subject-specific estimation of central aortic blood pressure using an individualized transfer function: a preliminary feasibility study.,” *IEEE Trans. Inf. Technol. Biomed.*, vol. 16, no. 2, pp. 212–20, Mar. 2012.

[35] G. Swamy, N. B. Olivier, and R. Mukkamala, “Calculation of forward and backward arterial waves by analysis of two pressure waveforms.,” *IEEE Trans. Biomed. Eng.*, vol. 57, no. 12, pp. 2833–9, Dec. 2010.

[36] G. Swamy, D. Xu, N. B. Olivier, and R. Mukkamala, “An adaptive transfer function for deriving the aortic pressure waveform from a peripheral artery pressure waveform.,” *Am. J. Physiol.*, vol. 297, no. 5, pp. H1956–63, Nov. 2009.

[37] M. Sugimachi, T. Shishido, K. Miyatake, and K. Sunagawa, “A new model-based method of reconstructing central aortic pressure from peripheral arterial pressure,” *Japan J. Physiol.*, vol. 51, pp. 217–222, 2001.

[38] T. J. Mullen, M. L. Appel, R. Mukkamala, J. M. Mathias, and R. J. Cohen, "System identification of closed-loop cardiovascular control: effects of posture and autonomic blockade," *Am. J. Physiol.*, vol. 272, pp. H448–461, 1997.

[39] J. Pan and W. J. Tompkins, "A real-time QRS detection algorithm.," *IEEE Trans. Biomed. Eng.*, vol. 32, no. 3, pp. 230–6, Mar. 1985.

[40] L. Ljung, *System Identification: Theory for the User*. Englewood Cliffs: Prentice Hall, 1987.

[41] R. Mukkamala, A. T. Reisner, H. M. Hojman, R. G. Mark, and R. J. Cohen, "Continuous cardiac output monitoring by peripheral blood pressure waveform analysis," *IEEE Trans. Bio-medical Eng. Biomed. Eng.*, vol. 53, pp. 459–467, 2006.

[42] D. Ross, *Animal Models in Cardiovascular Research*, 3td ed. Dordrecht; New York: Springer, 2009, pp. 135,137–138.

[43] Y. C. Chiu, P. W. Arand, S. G. Shroff, T. Feldman, and J. D. Carroll, "Determination of Pulse-Wave Velocities with Computerized Algorithms," *Am. Heart J.*, vol. 121, no. 5, pp. 1460–1470, 1991.

[44] E. Hermeling, K. D. Reesink, R. S. Reneman, and A. P. G. Hoeks□, "Measurements of local pulse wave velocity: effect of signal processing on precision," *Ultrasound Med. Biol*, vol. 33, no. 5, pp. 774–781, 2007.

[45] O. Vardoulis, T. G. Papaioannou, and N. Stergiopulos, "Validation of a novel and existing algorithms for the estimation of pulse transit time: advancing the accuracy in pulse wave velocity measurement.," *Am. J. Physiol. Heart Circ. Physiol.*, vol. 304, no. 11, pp. H1558–67, Jun. 2013.

[46] K. H. Parker, "An introduction to wave intensity analysis," *Med. Biol. Eng. Comput.*, vol. 47, no. 2, pp. 175–188, 2009.

[47] T. W. Latson, W. C. Hunter, N. Katoh, and K. Sagawa, "Effect of Nitroglycerin on Aortic Impedance, Diameter, and Pulse-Wave Velocity," *Circ. Res.*, vol. 62, no. 5, pp. 884–890, May 1988.

[48] R. M. Xu D. K. L. Ryan, C. A. Rickards, G. Zhang, V. A. Convertino, "Improved pulse transit time estimation by system identification analysis of proximal and distal arterial waveforms," *Am. J. Physiol.*, pp. 1389–1395, 2011.

[49] G. Zhang, J.-O. Hahn, and R. Mukkamala, "Tube-load model parameter estimation for monitoring arterial hemodynamics.," *Front. Physiol.*, vol. 2, no. November, p. 72, Jan. 2011.

[50] A. W. Khir and K. H. Parker, “Wave intensity in the ascending aorta: effects of arterial occlusion.,” *J. Biomech.*, vol. 38, no. 4, pp. 647–55, Apr. 2005.

[51] P. Segers and P. Verdonck, “Role of tapering in aortic wave reflection : hydraulic and mathematical model study,” *J. Biomech.*, vol. 33, pp. 299–306, 2000.

[52] M. F. Orourke and T. Yaginuma, “Wave Reflections and the Arterial Pulse,” *Arch. Intern. Med.*, vol. 144, no. 2, pp. 366–371, 1984.

[53] T. Weber, M. Ammer, M. Rammer, A. Adji, M. F. O’Rourke, S. Wassertheurer, S. Rosenkranz, and B. Eber, “Noninvasive determination of carotid-femoral pulse wave velocity depends critically on assessment of travel distance: a comparison with invasive measurement.,” *J. Hypertens.*, vol. 27, no. 8, pp. 1624–30, Aug. 2009.

[54] S. Laurent, J. Cockcroft, L. Van Bortel, P. Boutouyrie, C. Giannattasio, D. Hayoz, B. Pannier, C. Vlachopoulos, I. Wilkinson, H. Struijker-Boudier, and E. N. Non-invasive, “Expert consensus document on arterial stiffness: methodological issues and clinical applications,” *Eur. Heart J.*, vol. 27, no. 21, pp. 2588–2605, 2006.

[55] R. Mukkamala, J. Hahn, O. T. Inan, L. K. Mestha, C. Kim, and T. Hakan, “Toward Ubiquitous Blood Pressure Monitoring via Pulse Transit Time : Theory and Practice,” vol. 62, no. 8, pp. 1879–1901, 2015.

[56] X.-R. Ding, Y.-T. Zhang, J. Liu, W.-X. Dai, and H. K. Tsang, “Continuous Cuffless Blood Pressure Estimation Using Pulse Transit Time and Photoplethysmogram Intensity Ratio.,” *IEEE Trans. Biomed. Eng.*, vol. 9294, no. c, Sep. 2015.

[57] J. Solà, M. Proença, D. Ferrario, J. Porchet, A. Falhi, Y. Allemann, S. F. Rimoldi, and C. Sartori, “Non-invasive and non-occlusive blood pressure estimation via a chest sensor,” 2013, no. c.

[58] E. Hermeling, A. P. G. Hoeks, M. H. M. Winkens, J. L. Waltenberger, R. S. Reneman, A. a Kroon, and K. D. Reesink, “Noninvasive assessment of arterial stiffness should discriminate between systolic and diastolic pressure ranges.,” *Hypertension*, vol. 55, no. 1, pp. 124–30, Jan. 2010.

[59] E. Hermeling, S. J. Vermeersch, E. R. Rietzschel, M. L. de Buyzere, T. C. Gillebert, R. J. van de Laar, I. Ferreira, A. P. Hoeks, L. M. van Bortel, R. S. Reneman, P. Segers, and K. D. Reesink, “The change in arterial stiffness over the cardiac cycle rather than diastolic stiffness is independently associated with left ventricular mass index in healthy middle-aged individuals.,” *J. Hypertens.*, vol. 30, no. 2, pp. 396–402, Feb. 2012.

[60] M. Gao and R. Mukkamala, “Perturbationless Calibration of Pulse Transit Time to Blood Pressure,” 2012, pp. 232–235.

[61] M. Gao, G. Zhang, N. B. Olivier, and R. Mukkamala, “Improved Pulse Wave Velocity Estimation Using an Arterial Tube-Load Model,” vol. 61, no. 3, pp. 848–858, 2014.

[62] M. Remoissenet, *Waves Called Solitons. Concepts and Experiments*. Berlin: Springer-Verlag, 1994.

[63] S. Y. Lee and A. Konrad, “Lossy Transmission Line Transient Analysis by the Finite Element Method,” *IEEE Transation Magn.*, vol. 29, no. 2, pp. 1730–1732, 1993.

[64] S.-H. Sung, H.-M. Cheng, S.-Y. Chuang, Y.-T. Shih, K.-L. Wang, Y.-H. Chen, S.-J. Lin, W.-C. Yu, and C.-H. Chen, “Measurement of central systolic blood pressure by pulse volume plethysmography with a noninvasive blood pressure monitor.,” *Am. J. Hypertens.*, vol. 25, no. 5, pp. 542–8, May 2012.

[65] L. A. et al Geddes, “Pulse arrival time as a method of obtaining systolic and diastolic blood pressure indirectly,” no. September, pp. 671–672, 1981.

[66] R. Ochiai, H. Hosaka, Y. Sugo, and T. Soma, “THE RELATIONSHIP BETWEEN MODIFIED PULSE WAVE TRANSIT TIME AND CARDIOVASCULAR CHANGES IN ISOFLURANE ANESTHETIZED DOGS,” vol. 15, pp. 493–501, 1999.

[67] Y. Chen, C. Wen, G. Tao, M. Bi, and G. Li, “Continuous and noninvasive blood pressure measurement: a novel modeling methodology of the relationship between blood pressure and pulse wave velocity.,” *Ann. Biomed. Eng.*, vol. 37, no. 11, pp. 2222–33, Nov. 2009.

[68] C. C. Young, J. B. Mark, W. White, Y. Cc, M. Jb, W. White, A. Debree, V. Js, A. Fleming, A. Debree, J. S. Vender, and A. Fleming, “CLINICAL EVALUATION OF CONTINUOUS NONINVASIVE BLOOD PRESSURE MONITORING : ACCURACY AND TRACKING CAPABILITIES,” 1995.

[69] P. R. Painter, “The velocity of the arterial pulse wave: a viscous-fluid shock wave in an elastic tube.,” *Theor. Biol. Med. Model.*, vol. 5, p. 15, Jan. 2008.

[70] B. B. M. Learoyd, M. G. Taylor, and D. Ph, “Alterations with Age in the Viscoelastic Properties of Human Arterial Walls,” vol. 18, pp. 278–292, 1966.

[71] H. Cox, “Regional variation of series elasticity canine arterial smooth muscles,” no. 18, 1978.

[72] V. A. Convertino, W. H. Cooke, and J. B. Holcomb, “Arterial pulse pressure and its association with reduced stroke volume during progressive central hypovolemia,” *J. Trauma*, vol. 61, pp. 629–634, 2006.

[73] “(2011). Using the pulse oximeter: Tutorial 2, advanced.” [Online]. Available: http://www.who.int/patientsafety/safesurgery/pulse_oximetry/.

[74] M. Karamanoglu, M. F. O'Rourke, A. P. Avolio, and R. P. Kelly, "An analysis of the relationship between central aortic and peripheral upper limb pressure waves in man," *Eur. Hear. J.*, vol. 14, pp. 160–167, 1993.

[75] C. H. Chen, E. Nevo, B. Fetics, P. H. Pak, F. C. Yin, W. L. Maughan, and D. A. Kass, "Estimation of central aortic pressure waveform by mathematical transformation of radial tonometry pressure. Validation of generalized transfer function," *Circulation*, vol. 95, pp. 1827–1836, 1997.

[76] B. Fetics, E. Nevo, C. H. Chen, and D. A. Kass, "Parametric model derivation of transfer function for noninvasive estimation of aortic pressure by radial tonometry," *Ieee Trans. Biomed. Eng.*, vol. 46, no. 6, pp. 698–706, 1999.

[77] and J. S. Kiichi Sagawa, Reidar K. Lie, "Translation of Otto Frank ' s Paper 'Die Grundform des Arteriellen Pulses' Zeitschrift fur Biologie 37: 483-526 (1899)," *J Mul Cell Cardiol*, vol. 22, pp. 253–254, 1990.

[78] J. E. H. Arthur C. Guyton, *Textbook of Medical Physiology*, 11th ed. Elsevier, 2006, p. 173.

[79] M. J. Bourgeois, B. K. Gilbert, D. E. Donald, and E. H. Wood, "Characteristics of aortic diastolic pressure decay with application to the continuous monitoring of changes in peripheral vascular resistance," *Circ. Res.*, vol. 35, pp. 56–66, 1974.

[80] M. Malik, "If Dr. Bazett had had a computer...," *PACE*, vol. 19, pp. 1635–1639, 1996.

[81] S. Holm, "A simple sequentially rejective multiple test procedure," vol. 6, pp. 65–70, 1979.

[82] R. Mukkamala and M. Gao, "A Comparative Analysis of Reduced Arterial Models for Hemodynamic Monitoring," pp. 225–228, 2013.

[83] "Sphygmocor New Population Reference Data," 2016. [Online]. Available: http://www.atcormedical.com/pdf/TN15 - New Population Reference Data.pdf.

[84] D. Agnoletti, Y. Zhang, P. Salvi, C. Borghi, J. Topouchian, M. E. Safar, and J. Blacher, "Pulse pressure amplification, pressure waveform calibration and clinical applications.," *Atherosclerosis*, vol. 224, no. 1, pp. 108–12, Sep. 2012.

[85] Y.-T. Shih, H.-M. Cheng, S.-H. Sung, W.-C. Hu, and C.-H. Chen, "Quantification of the Calibration Error in the Transfer Function-Derived Central Aortic Blood Pressures.," *Am. J. Hypertens.*, vol. 24, no. 12, pp. 1312–7, Dec. 2011.

[86] H.-M. Cheng, D. Lang, C. Tufanaru, and A. Pearson, "Measurement Accuracy of non-invasively obtained central blood pressure by applanation tonometry: a systematic review and meta-analysis.," *Int. J. Cardiol.*, vol. 167, no. 5, pp. 1867–76, Sep. 2013.

[87] E. Agabiti-Rosei, G. Mancia, M. F. O'Rourke, M. J. Roman, M. E. Safar, H. Smulyan, J. G. Wang, I. B. Wilkinson, B. Williams, and C. Vlachopoulos, "Central blood pressure measurements and antihypertensive therapy a consensus document," *Hypertension,* vol. 50, no. 1, pp. 154–160, 2007.

[88] R. Pini, M. C. Cavallini, V. Palmieri, N. Marchionni, M. Di Bari, R. B. Devereux, G. Masotti, and M. J. Roman, "Central but not brachial blood pressure predicts cardiovascular events in an unselected geriatric population," *J. Am. Coll. Cardiol.*, vol. 51, no. 25, pp. 2432–2439, 2008.